

# TACTiS: Transformer-Attentional Copulas for Time Series

Alexandre Drouin <sup>\*†</sup> Étienne Marcotte <sup>\*†</sup> Nicolas Chapados <sup>\*†</sup>

## Abstract

The estimation of time-varying quantities is a fundamental component of decision making in fields such as healthcare and finance. However, the practical utility of such estimates is limited by how accurately they quantify predictive uncertainty. In this work, we address the problem of estimating the joint predictive distribution of high-dimensional multivariate time series. We propose a versatile method, based on the transformer architecture, that estimates joint distributions using an attention-based decoder that provably learns to mimic the properties of non-parametric copulas. The resulting model has several desirable properties: it can scale to hundreds of time series, supports both forecasting and interpolation, can handle unaligned and non-uniformly sampled data, and can seamlessly adapt to missing data during training. We demonstrate these properties empirically and show that our model produces state-of-the-art predictions on several real-world datasets.

## 1. Introduction

In numerous time series forecasting contexts, data presents itself in a raw form that rarely matches the standard assumptions of classical forecasting methods. For instance, in healthcare settings and economic forecasting, groups of related time series can have different sampling frequencies, be sampled irregularly, and exhibit missing values (Shukla & Marlin, 2021b; Sun et al., 2020). Covariates that are predictive of future behavior may not be available for all historical data, or may be available in a different form.<sup>1</sup> Moreover, optimal decision-making in downstream tasks generally requires the full joint predictive distribution over arbitrary future time horizons (Peterson, 2017), not just marginal quantiles thereof at a fixed horizon. We seek to develop general forecasting methods that are both suitable for a wide range of downstream tasks and that can handle all stylized facts about real-world

<sup>\*</sup>Equal contribution <sup>†</sup>ServiceNow Research. Correspondence to: All authors <firstname.lastname@servicenow.com>.

Preprint, under review.

<sup>1</sup>E.g., due to changes in the measurement methodology.

time series—as they are, not as they ought to be—namely:

- Joint characterization of a multivariate stochastic process, forecasting trajectories at arbitrary time horizons.
- Presence of observed (non-stochastic) covariates, either static or time-varying, used as conditioning variables.
- Variables within the process that are measured at different sampling frequencies, or irregularly sampled.
- Missing values for arbitrary time points and variables in the process.
- Variables with different domains— $\mathbb{R}, \mathbb{R}^+, \mathbb{N}, \mathbb{N}^+, \mathbb{Z}$ —with skewed and fat-tailed marginal behavior.

Classical times series models, such as ARIMA (Box et al., 2015) and exponential smoothing methods (Hyndman et al., 2008), are very restricted in their handling of the above stylized facts. Although extensions have been proposed that deal with individual issues, they cannot easily deal with all and require considerable domain knowledge to be effective. Machine learning models have recently gained in popularity (Benidis et al., 2020). Nevertheless, methods introduced in recent years all suffer from limitations when dealing with one or more of the above listed stylized facts, or neglect in their handling of the full predictive distribution.

Separately, multivariate forecasting models based on copulas have been popular in econometrics for more than a decade (Patton, 2012; Rémillard et al., 2012; Krupskii & Joe, 2020; Mayer & Wied, 2021). These models enable the separate characterization of the joint behavior of a group of random variables from their marginal behavior. This has been found to be especially valuable in areas such as finance and insurance where marginals are known to exhibit particular patterns of skewness and kurtosis. Recently in machine learning, low-rank Gaussian copula processes with LSTMs (Hochreiter & Schmidhuber, 1997) have been proposed for high-dimensional forecasting (Salinas et al., 2019).

Building on the recent successes of transformers as general-purpose sequence models (Vaswani et al., 2017) and their success in time series forecasting (Rasul et al., 2021b; Tashiro et al., 2021; Tang & Matteson, 2021), we propose a transformer architecture that can tackle all the above stylized facts about real-world time series. Notably, we show how to represent an implicit copula when sampling from the transformer decoder model. Moreover, by representing each observation as having its own timestamp, we can naturally

handle irregularly sampled times series as well as series with missing values and unequal sampling frequencies. We also show that an efficient two-dimensional attention scheme lets us scale to hundreds of time steps and series using vanilla attention (Bahdanau et al., 2015).

### Contributions:

1. We present *Transformer-Attentional Copulas for Time Series* (TACTiS), a highly flexible transformer-based model for large-scale multivariate probabilistic time series prediction (§4).
2. We introduce *attentional copulas*, an attention-based architecture that estimates non-parametric copulas for an arbitrary number of random variables (§4.2).
3. We theoretically prove the convergence of attentional copulas to valid copulas (§4.3).
4. We conduct an empirical study showing TACTiS’ state-of-the-art probabilistic prediction performance on several real-world datasets, along with great flexibility (§5).

## 2. Background

### 2.1. Problem setting

We are interested in the general problem of estimating the joint distribution of values missing at arbitrary time points in multivariate time series. This general task encompasses classical problems, such as probabilistic forecasting, backcasting, and interpolation.

Formally, we consider a set of  $m$  multivariate time series  $\mathcal{S} \stackrel{\text{def}}{=} \{\mathbf{X}_1, \dots, \mathbf{X}_m\}$ , where each  $\mathbf{X} \in \mathcal{S}$  is a collection of possibly-related univariate time series. For simplicity, we elaborate the notation for a single element of  $\mathcal{S}$ . Let  $\mathbf{X} \stackrel{\text{def}}{=} \{\mathbf{x}_i \in \mathbb{R}^{l_i}\}_{i=1}^n$ , where the  $\mathbf{x}_i$  are univariate time series with arbitrary lengths  $l_i \in \mathbb{N}^+$ . Each  $\mathbf{x}_i$  is associated with (i) a Boolean mask  $\mathbf{m}_i \in \mathbb{B}^{l_i}$ , such that  $m_{ij} = 1$  if  $x_{ij}$  is observed and  $m_{ij} = 0$  otherwise, (ii) a matrix of time-varying covariates  $\mathbf{C}_i \stackrel{\text{def}}{=} [\mathbf{c}_{i1}, \dots, \mathbf{c}_{il_i}] \in \mathbb{R}^{l_i \times d}$ , which represent arbitrary additional information, and (iii) a vector of time stamps  $\mathbf{t}_i \in \mathbb{R}^{l_i}$  s.t.  $t_{ij} < t_{i,j+1}$ , indicating the times at which the data were measured. Note that this setting naturally supports unaligned time series with arbitrary sampling frequencies.

Our goal is to infer the joint distribution of missing time series values given all known information:<sup>2</sup>

$$P\left(\left\{\mathbf{x}_i^{(m)}\right\}_{i=1}^n \mid \left\{\mathbf{x}_i^{(o)}, \mathbf{C}_i, \mathbf{t}_i\right\}_{i=1}^n\right), \quad (1)$$

where  $\mathbf{x}_i^{(o)}$  and  $\mathbf{x}_i^{(m)}$  are the observed ( $m_{ij} = 1$ ) and missing ( $m_{ij} = 0$ ) elements of  $\mathbf{x}_i$ , respectively.

From this problem formulation, one can recover standard time series problems via specific masking patterns. For

instance, a  $t$ -step probabilistic forecasting task can be defined by setting the last  $t$  elements of each  $\mathbf{m}_i$  to zero.

### 2.2. Transformers

The model that we propose builds on the *transformer architecture* for sequence-to-sequence transduction (Vaswani et al., 2017). Transformer models have an encoder-decoder structure, where the encoder learns a representation of the tokens of an input sequence, and the decoder generates the tokens of an output sequence autoregressively, based on the input sequence. The main feature of such models is that they can capture non-sequential dependencies between tokens via attention mechanisms (Bahdanau et al., 2015). This is in sharp contrast with recurrent neural networks (Goodfellow et al., 2016), such as LSTMs (Hochreiter & Schmidhuber, 1997), which are inherently sequential. Transformers have been widely discussed in the literature and thus, we refer the reader to the seminal work of Vaswani et al. (2017) for additional details. As we later describe, transformers allow TACTiS to view time series as sets of tokens, among which non-local dependencies can be learned regardless of considerations like alignment and sampling frequency.

### 2.3. Copulas

Copulas are mathematical constructs that allow separating the joint dependency structure of a set of random variables from their marginal distributions (Nelsen, 2007). Such a separation can be used to learn reusable models that can be applied to seemingly different distributions, where variables have different marginals, but the same dependency structure.

Formally, a copula  $C : [0, 1]^d \rightarrow [0, 1]$  is the joint cumulative distribution function (CDF) of a  $d$ -dimensional random vector  $[U_1, \dots, U_d]$  on the unit cube with uniform marginal distributions, i.e.,

$$C(u_1, \dots, u_d) \stackrel{\text{def}}{=} P(U_1 \leq u_1, \dots, U_d \leq u_d), \quad (2)$$

where  $U_i \sim U_{[0,1]}$ . According to Sklar (1959)’s theorem, the joint CDF of any random vector  $[X_1, \dots, X_d]$  can be expressed as a combination of a copula  $C$  and the marginal CDF of each random variable  $F_i(x_i) \stackrel{\text{def}}{=} P(X_i \leq x_i)$ ,

$$P(X_1 \leq x_1, \dots, X_d \leq x_d) = C(F_1(x_1), \dots, F_d(x_d)), \quad (3)$$

and the corresponding probability density<sup>3</sup> is given by:

$$p(X_1 = x_1, \dots, X_d = x_d) = c(F_1(x_1), \dots, F_d(x_d)) \times f_1(x_1) \times \dots \times f_d(x_d), \quad (4)$$

where  $c : [0, 1]^d \rightarrow [0, 1]$  is the copula’s density function and the  $f_i$  are the marginal density functions of the  $X_i$ .

<sup>2</sup>We slightly abuse the notation and omit random variables.

<sup>3</sup>Assuming that the distribution is continuous.

It is thus possible to estimate seemingly complex joint distributions by learning the parameters of a simple internal joint distribution (the copula) and marginal distributions, which can even be estimated empirically. One classical approach, which has been used abundantly in time series applications is the Gaussian copula (Nelsen, 2007), where  $C$  is constructed using a Gaussian distribution.

In this work, we avoid making such parametric assumptions and propose a new attention-based architecture trained to mimic a non-parametric copula, which we term *attentional copula*. TACTiS learns to produce the parameters of the copula, on-the-fly, based on learned variable representations. It can thus reuse a learned dependency structure across multiple sets of variables, by learning to map them to similar representations.

### 3. Related work

**Neural Networks for Time Series Forecasting** Although studied in the 1990’s (Zhang et al., 1998), neural networks and other machine learning (ML) techniques had long been taken with caution in the forecasting community due to a perceived propensity to overfit (Makridakis et al., 2018). In recent years, however, the field has seen a number of demonstrations of successful ML-based forecasting, in particular, winning the prestigious M5 competition (Makridakis et al., 2021; 2022). For neural networks, work has mostly centered around so-called global models (Montero-Manso & Hyndman, 2021), which in contrast to classical statistical methods such as ARIMA (Box et al., 2015) or exponential smoothing (Hyndman et al., 2008), learn a single set of parameters to forecast many series. A first wave of approaches in the recent resurgence was primarily based on recurrent or convolutional neural network encoders (Shih et al., 2019; Chen et al., 2020). Oreshkin et al. (2020) introduce a recursive decomposition based on a residual signal projection on a set of learned basis functions. Le Guen & Thome (2020) introduce an approach for univariate probabilistic forecasting based on determinantal point processes to capture structured shape and temporal diversity. Extensions of classical state-space models have also been proposed (Yanchenko & Mukherjee, 2020; de Bézenac et al., 2020). Comprehensive surveys of deep learning methods for forecasting appear in Lim & Zohren (2021) and Benidis et al. (2020), restricting coverage to regularly-sampled data. Of relevance to the present work are studies of probabilistic multivariate methods, transformer-based approaches, copulas, and techniques enabling irregular sampling.

**Probabilistic Multivariate Methods** Narrowing attention to methods carrying out probabilistic forecasting of the joint distribution of a multivariate stochastic process, DeepAR (Salinas et al., 2020) computes an iterated one-step-ahead Monte Carlo approximation of the predictive distribution

by sampling from a fixed functional form whose parameters are the result of a recurrent neural network (RNN). Likewise, Rasul et al. (2021a) propose instead to model the predictive joint one-step-ahead distribution using a denoising diffusion process (Ho et al., 2020; Sohl-Dickstein et al., 2015); however, with the diffusion dynamics conditioned on an RNN, the model cannot easily deal with missing values or irregularly sampled time series. Rasul et al. (2021b) propose to model the predictive joint one-step-ahead distribution by a multivariate normalizing flow (Papamakarios et al., 2021), parametrized by either a RNN or a transformer.

**Transformer-based approaches** have come to the fore more recently, on the strength of their successes in other sequence modeling tasks. Lim et al. (2021) introduce the temporal fusion transformer, combining recurrent layers for local processing and self-attention layers for characterizing long-term dependencies, evaluating performance on quantile loss measures; notably, the architecture makes use of a gating mechanism to suppress unnecessary covariates. Li et al. (2019) introduce a transformer with subquadratic memory complexity along with convolutional self-attention to better handle local context. Spadon et al. (2021) propose a recurrent graph evolution neural networks, which embeds transformers, to carry out point multivariate forecasting. Tashiro et al. (2021) use a conditional score-based diffusion model explicitly trained for interpolation and report substantial improvements over existing probabilistic imputation models, as well as competitive performance on some forecasting tasks against recently-proposed deep learning models. Tang & Matteson (2021) introduce a variational non-Markovian state space model where the latent dynamics are given by an attention mechanism over all previous latents and observed tokens. They report good multivariate probabilistic forecasting results on five standard datasets, as well as on the task of human motion prediction. Recently, outside of time series forecasting, Müller et al. (2022) show how to train a transformer-based model to approximate the Bayesian posterior predictive distribution in regression tasks; these results are in the spirit of the forecasting and interpolation results that we present in this paper.

**Copulas-Based Forecasting** There exists an abundant literature on uses of copulas (Größer & Okhrin, 2021) for economic and financial forecasting, although most published models have focused on fixed functional forms (Patton, 2012; Rémillard et al., 2012). Aas et al. (2009) introduce vine copulas that provide increased pairwise flexibility, and Krupskii & Joe (2020); Mayer & Wied (2021) suggest more flexible forms for forecasting applications. In ML, Lopez-Paz et al. (2012) propose to carry out domain adaptation using a form of non-parametric copulas based on kernel estimators. For forecasting, Salinas et al. (2019) introduce GPVar, an LSTM-based method that dynamically parametrizes a Gaussian copula. To the best of our knowledge, none of the published meth-

ods show how to sample from a *non-parametric copula* resulting from an autoregressive decomposition of a time-varying conditional copula distribution, as we introduce in this work.

**Irregular Sampling** Gaussian processes have been widely used to handle irregularly-sampled series (Williams & Rasmussen, 2006; Chapados & Bengio, 2007), but these approaches are limited in other ways, notably in tractability. More recently, Shukla & Marlin (2021a) have proposed a transformer-like attention mechanism to re-represent an irregularly sampled time series at a fixed set of reference points, and evaluate on interpolation and classification tasks.

## 4. The TACTiS model

Our contribution is a flexible model for multivariate probabilistic time series prediction composed of a transformer encoder (Vaswani et al., 2017) and an attention-based decoder trained to mimic a non-parametric copula; hence the name *Transformer-Attentional Copulas for Time Series* (TACTiS). Fig. 1 shows an overview of the model architecture<sup>4</sup>.

Akin to classical Transformers (Vaswani et al., 2017), TACTiS views the elements of a multivariate time series ( $x_{ij}$ ) as an arbitrary set of tokens, where some tokens are observed and some are missing (based on  $m_{ij}$ ). The encoder is tasked with learning a meaningful representation of each token, such as to enable the decoder to infer a multivariate joint distribution over the values of the missing tokens. Due to the use of attention in both the encoder and the decoder, TACTiS can adapt to an arbitrary number of tokens, without retraining.

TACTiS learns the conditional predictive distribution of arbitrary missing values in multivariate time series. At inference time, it is the pattern of missing values themselves—namely, where they are located with respect to measured values—that determines whether it performs forecasting, interpolation, or another similar task. Consequently, TACTiS naturally supports changes in its inputs, such as the unavailability of some time series, and in its outputs, such as changes in forecast horizon. Moreover, it inherently supports misalignment and differences in sampling frequencies, since each token is encoded separately. This is in sharp contrast with classical vector autoregressive models (Wei, 2018) and most recurrent neural networks, which jointly consider the values of each time series at a given time step ( $j$ ) as a vector  $(x_{1j}, \dots, x_{nj}) \in \mathbb{R}^n$ . We now detail the encoder, decoder, training procedure, and provide some theoretical guarantees.

### 4.1. Encoder

As shown in Fig. 1, the encoder used in TACTiS is identical to that of standard Transformers (Vaswani et al., 2017), except that all tokens (observed and missing) are encoded

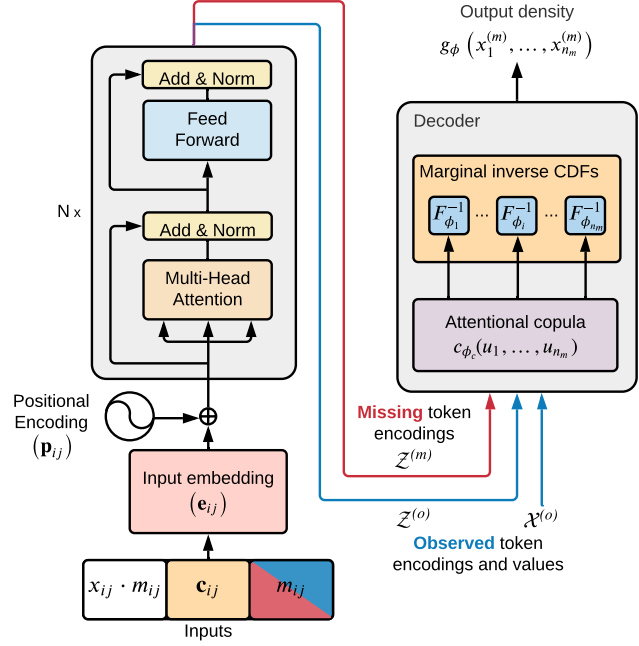


**Figure 1:** Model overview. **(Left)** The TACTiS encoder is very similar to that of standard transformers. The key difference is that both observed and missing tokens are encoded simultaneously. **(Right)** The decoder, based on an attentional copula, learns the output density given representations of the observed and missing tokens.

simultaneously.

**Input embedding** The encoder starts by producing a vector embedding ( $\mathbf{e}_{ij} \in \mathbb{R}^{d_{\text{emb}}}$ ) for each element in each time series (i.e., tokens), which accounts for its value  $x_{ij}$ , the associated covariates<sup>5</sup>  $\mathbf{c}_{ij}$  and whether it is observed or missing  $m_{ij}$ . Such embeddings are given by a neural network with parameters  $\theta_{\text{emb}}$ , with  $x_{ij} \cdot m_{ij}$  masking the values of missing tokens:

$$\mathbf{e}_{ij} = \text{Embed}_{\theta_{\text{emb}}}(x_{ij} \cdot m_{ij}, \mathbf{c}_{ij}, m_{ij}).$$

**Positional encoding** We add information about a token’s time stamp  $t_{ij}$  to the input embedding via a positional encoding  $\mathbf{p}_{ij} \in \mathbb{R}^{d_{\text{emb}}}$ . For simplicity, we use the positional encodings of Vaswani et al. (2017), based on sine and cosine functions of various frequencies, and obtain the final embeddings as  $\mathbf{e}'_{ij} = \mathbf{e}_{ij} \sqrt{d_{\text{emb}}} + \mathbf{p}_{ij}$ . Note that other choices, such as positional encodings tailored to time series (e.g., accounting for holidays, day of week, etc.), would be viable, but we keep such explorations for future work.

Then, following Vaswani et al. (2017), the  $\mathbf{e}'_{ij}$  embeddings are passed through a stack of residual layers that combine multi-head self-attention and layer normalization to obtain an encoding ( $\mathbf{z}_{ij}$ ) for each token. Such encodings contain a complex mixture of information from other tokens that were deemed relevant by the attention mechanism, such as

<sup>4</sup>An implementation will be made available upon acceptance.

<sup>5</sup> Optionally, we include a learned, per series, embedding in  $\mathbf{c}_{ij}$ .

the value of their covariates, their time stamp, and the values of observed tokens.

**Scalability** One well-known limitation of transformers is the large time and memory complexity of self-attention, scaling quadratically with the number of tokens. However, improving the efficiency of transformers is an active field of research (Tay et al., 2020; Lin et al., 2021) and any progress in this direction is poised to be directly applicable to TACTiS. In this work, when applying TACTiS to large datasets, such as those in § 5, we take advantage of the fact that each token is indexed by two independent indices:  $i$  for the variables, and  $j$  for the time steps. We do so by employing the temporal transformer layers of Tashiro et al. (2021), which first compute self-attention between the tokens of each variable ( $x_{i1}, \dots, x_{il_i}$ ) and then between the tokens at a given time step ( $x_{1j}, \dots, x_{nj}$ ). Hence, instead of scaling in  $O([n \cdot l_{\max}]^2)$ , the time and memory complexity scale in  $O(n^2 \cdot l_{\max} + n \cdot l_{\max}^2)$ , where  $n$  is the number of time series and  $l_{\max} \stackrel{\text{def}}{=} \max_i l_i$  is the length of the longest time series. One downside of this approach is that, for attention within a given time step ( $j$ ) to make sense, the time series must be aligned. When this type of attention is used, we will refer to our model as TACTiS-TT (for Temporal Transformer).

## 4.2. Decoder

As stated in Eq. (1), we aim to learn the joint distribution of the values ( $x_{ij}$ ) of missing tokens ( $m_{ij} = 0$ ), given the values of observed tokens ( $m_{ij} = 1$ ), the covariates ( $\mathbf{c}_{ij}$ ), and the time stamps ( $t_{ij}$ ). We achieve this via an attention-based decoder trained to mimic a non-parametric copula (see §2.3), which we now describe.

Since the data consists of an arbitrary set of observed and missing tokens, we introduce the following notation:  $\mathcal{Z}^{(o)} \stackrel{\text{def}}{=} \{\mathbf{z}_1^{(o)}, \dots, \mathbf{z}_{n_o}^{(o)}\}$  and  $\mathcal{Z}^{(m)} \stackrel{\text{def}}{=} \{\mathbf{z}_1^{(m)}, \dots, \mathbf{z}_{n_m}^{(m)}\}$ , which respectively denote the encoded representations of observed and missing tokens. We also use  $\mathcal{X}^{(o)} \stackrel{\text{def}}{=} \{x_1^{(o)}, \dots, x_{n_o}^{(o)}\}$  and  $\mathcal{X}^{(m)} \stackrel{\text{def}}{=} \{x_1^{(m)}, \dots, x_{n_m}^{(m)}\}$  to denote the values of observed and missing tokens, respectively. Finally, we use  $\mathcal{C} \stackrel{\text{def}}{=} \{\mathbf{C}_1, \dots, \mathbf{C}_n\}$  and  $\mathcal{T} \stackrel{\text{def}}{=} \{\mathbf{t}_1, \dots, \mathbf{t}_n\}$  to denote the set of all covariates and timestamps, respectively.

Our goal is to accurately estimate the joint density of missing token values, using a model  $g_\phi(x_1^{(m)}, \dots, x_{n_m}^{(m)})$  such that:

$$g_\phi(x_1^{(m)}, \dots, x_{n_m}^{(m)}) \approx p(x_1^{(m)}, \dots, x_{n_m}^{(m)} | \mathcal{X}^{(o)}, \mathcal{C}, \mathcal{T}),$$

where the distributional parameters<sup>6</sup>  $\phi$  are produced by a neural network parametrized by  $\theta_{\text{dec}}$ :

$$\phi = \text{Decoder}_{\theta_{\text{dec}}}(\mathcal{X}^{(o)}, \mathcal{Z}^{(o)}, \mathcal{Z}^{(m)}).$$

<sup>6</sup>We use subscripted versions of  $\phi$  and  $\theta$  to denote distributional parameters and neural network parameters, respectively.

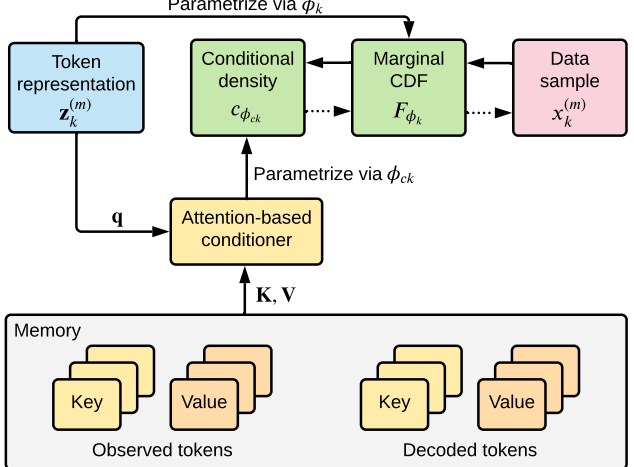


**Figure 2:** Overview of the TACTiS decoder architecture. Dotted arrows indicate the flow of information during sampling.

We consider the following copula-based structure for  $g_\phi$ :

$$\begin{aligned} g_\phi(x_1^{(m)}, \dots, x_{n_m}^{(m)}) &\stackrel{\text{def}}{=} \\ c_{\phi_c} \left( F_{\phi_1}(x_1^{(m)}), \dots, F_{\phi_{n_m}}(x_{n_m}^{(m)}) \right) \\ &\times f_{\phi_1}(x_1^{(m)}) \times \dots \times f_{\phi_{n_m}}(x_{n_m}^{(m)}), \end{aligned} \quad (5)$$

where  $\phi \stackrel{\text{def}}{=} \{\phi_c, \phi_1, \dots, \phi_{n_m}\}$ ,  $c_{\phi_c}$  is the density of a copula, and the  $F_{\phi_k}$  and  $f_{\phi_k}$  represent the marginal CDF and density of  $X_k^{(m)}$  respectively.

The structure of  $g_\phi$  allows for a wealth of different copula parametrizations (e.g., the Gaussian copula of Salinas et al. (2019)). The crux of TACTiS resides in how each of the components is parametrized. Notably, we propose to use normalizing flows (Tabak & Turner, 2013) to model the marginals, and we develop a flexible non-parametric copula that can automatically adapt to a changing number of missing tokens ( $n_m$ ). We now outline these constructs, with an overview of the decoder architecture appearing in Fig. 2.

**Marginal distributions** To model the marginal CDFs ( $F_{\phi_k}$ ), we seek a function that (i) maps values to  $[0, 1]$ , (ii) is monotonically increasing, (iii) is both continuous and differentiable. We achieve this using a modified version of the Deep Sigmoidal Flows (DSF) of Huang et al. (2018), where we simply remove the logit function of the last flow layer to obtain values in  $[0, 1]$ . The parameters of each flow are produced by a neural network with parameters  $\theta_F$ , which are shared across all  $k$ ,

$$\phi_k = \text{MarginalParams}_{\theta_F}(\mathbf{z}_k^{(m)}). \quad (6)$$

The marginal densities  $f_{\phi_k}$  are obtained by differentiating  $F_{\phi_k}$  w.r.t.  $x_k^{(m)}$ , an efficient operation for DSF. In addition to satisfying our desiderata, DSFs have been shown to be

universal density approximators, thereby not constraining the modeling ability of TACTiS.

**Copula density** According to the definition of a copula, we must parametrize a distribution on the unit cube  $[0, 1]^{n_m}$  with uniform marginals. We consider an autoregressive factorization of the copula density according to an arbitrary permutation  $\pi = [\pi_1, \dots, \pi_{n_m}]$  of the indices  $\{1, \dots, n_m\}$ . We denote the copula density and its parameters by  $c_{\phi_c^\pi}$ :

$$\begin{aligned} c_{\phi_c^\pi}(u_1, \dots, u_{n_m}) = \\ c_{\phi_{c1}^\pi}(u_{\pi_1}) \times c_{\phi_{c2}^\pi}(u_{\pi_2} | u_{\pi_1}) \times \dots \times \\ c_{\phi_{cn_m}^\pi}(u_{\pi_{n_m}} | u_{\pi_1}, \dots, u_{\pi_{n_m-1}}), \end{aligned} \quad (7)$$

where  $c_{\phi_{ck}^\pi}$  is  $k^{\text{th}}$  conditional density in the factorization and  $u_{\pi_k} = F_{\phi_k}(x_{\pi_k}^{(m)})$ . Importantly, we let  $c_{\phi_{c1}^\pi}$  be the density of a uniform distribution  $U_{[0,1]}$  and use an *attention-based conditioner* to obtain the parameters of the remaining conditional distributions  $\phi_{ck}^\pi$ , for  $k > 1$ . We call the resulting construct an *attentional copula*.

**Attention-based conditioner** This component of the decoder produces the parameters  $\phi_{ck}^\pi$  for the conditional density  $c_{\phi_{ck}^\pi}(u_{\pi_k} | u_{\pi_1}, \dots, u_{\pi_{k-1}})$  by performing attention over a memory composed of the representations of observed tokens and missing tokens that are predecessors in the permutation:  $\{\mathbf{z}_1^{(o)}, \dots, \mathbf{z}_{n_o}^{(o)}, \mathbf{z}_{\pi_1}^{(m)}, \dots, \mathbf{z}_{\pi_{k-1}}^{(m)}\}$ , as well as their CDF-transformed<sup>7</sup> values  $\{u_1^{(o)}, \dots, u_{n_o}^{(o)}, u_{\pi_1}^{(m)}, \dots, u_{\pi_{k-1}}^{(m)}\}$ . The conditioner is composed of several layers, which are as follows. First, we calculate keys and values<sup>8</sup> for each element  $(\mathbf{z}, u)$  in the memory using two modules parametrized by  $\theta_k$  and  $\theta_v$ , respectively:

$$\mathbf{k} = \text{Key}_{\theta_k}(\mathbf{z}, u) \quad \mathbf{v} = \text{Value}_{\theta_v}(\mathbf{z}, u), \quad (8)$$

where  $\mathbf{k} \in \mathbb{R}^{d_{\text{att}}}$  and  $\mathbf{v} \in \mathbb{R}^{d_{\text{val}}}$ . We then calculate a query for our token of interest  $\mathbf{z}_{\pi_k}^{(m)}$  using a module with parameters  $\theta_q$

$$\mathbf{q} = \text{Query}_{\theta_q}(\mathbf{z}_{\pi_k}^{(m)}), \quad (9)$$

where  $\mathbf{q} \in \mathbb{R}^{d_{\text{att}}}$ . Let  $\mathbf{K}$  and  $\mathbf{V}$  be the matrices of all keys and values for tokens in the memory, respectively. Following Vaswani et al. (2017), we obtain an attention-based representation  $\mathbf{z}' \in \mathbb{R}^{d_{\text{att}}}$ :

$$\mathbf{z}' = \text{LayerNorm}(\mathbf{V}^\top \text{Softmax}(\mathbf{K}\mathbf{q}) + \text{Reshape}_{\theta_s}(\mathbf{z}_{\pi_k}^{(m)})),$$

where  $\text{Reshape}_{\theta_s}$  is a module that projects  $\mathbf{z}_{\pi_k}^{(m)}$  to  $\mathbb{R}^{d_{\text{att}}}$ . We repeat this process from Eq. (8) for each layer, with different parameters, and replacing  $\mathbf{z}_{\pi_k}^{(m)}$  by the output  $\mathbf{z}'$  of

<sup>7</sup>For observed tokens, transformation via the normalizing flow does not necessarily correspond to a CDF transform, but it ensures that all values are on a similar scale.

<sup>8</sup>For simplicity, we use a single attention head in the presentation, but in practice, we use multiple (see Vaswani et al. (2017)).

the previous layer. Finally, we obtain the parameters of the conditional distribution using a module parameterized by  $\theta_{\text{dist}}$  applied to the  $\mathbf{z}'$  of the last layer:

$$\phi_{ck}^\pi = \text{DistParams}_{\theta_{\text{dist}}}(\mathbf{z}').$$

**Choice of distribution** Any distribution with support  $[0, 1]$  can be used to model the conditional distributions  $c_{\phi_{ck}^\pi}^\pi$ . We choose to use a piecewise constant distribution, i.e., we divide the support into a number of bins, each parametrized by a probability density that applies to all the points it contains. Such a distribution can approximate complex multimodal distributions on  $[0, 1]$  without making parametric assumptions, similarly to van den Oord et al. (2016). The number of bins controls the level of approximation and is a hyperparameter. Among other valid choices are the Beta distribution and mixtures thereof.

**Sampling** We first draw a sample from the copula, autoregressively, following an arbitrary permutation  $\pi$ . Then, we transform each of the sampled values using their corresponding inverse marginal CDF, i.e.,  $F_{\phi_k}^{-1}(u_k^{(m)})$ . As per the definition of attentional copulas, the first element of the permutation is always sampled from a  $U_{[0,1]}$ . The fact that DSFs are invertible functions makes this possible (see §B.2 for details).

This concludes the presentation of the decoder. However, one question remains: what guarantees that  $c_{\phi_c^\pi}$  will converge to a valid copula? The key is in the training procedure.

### 4.3. Training procedure

Let  $g_{\phi^\pi}$  be the density estimator described in Eq. (5), where the copula is factorized according to permutation  $\pi$ . Let  $\Theta \stackrel{\text{def}}{=} \{\theta_{\text{enc}}, \theta_{\text{dec}}\}$  be the set containing the parameters of all the components of the encoder and the decoder, respectively. We obtain  $\Theta$  by minimizing the expected negative log-likelihood of our model over permutations  $\Pi$  and samples drawn from the set of all time series  $\mathcal{S}$ :

$$\underset{\Theta}{\operatorname{argmin}} \mathbb{E}_{\substack{\pi \sim \Pi \\ \mathbf{X} \sim \mathcal{S}}} - \log g_{\phi^\pi}(x_1^{(m)}, \dots, x_{n_m}^{(m)}). \quad (10)$$

**Theorem 4.1.** *The copula  $c_{\phi_c^\pi}$  embedded in a density estimator  $g_{\phi^\pi}$ , as shown in Eq. (5), with distributional parameters  $\phi^\pi$  given by a decoder with parameters by  $\theta_{\text{dec}} \in \Theta$ , where  $\Theta$  minimizes Eq. (10), is a valid copula.*

*Proof.* The proof, given in § A, relies on the fact that optimizing Eq. (10) leads to permutation invariance which, by the definition of  $c_{\phi_{c1}^\pi}$ , results in uniform marginals. The resulting copula  $c_{\phi_c^\pi}$  is therefore a valid copula.  $\square$

Hence, TACTiS provably learns to disentangle the joint dependency structure of random variables from their marginal

distributions via flexible non-parametric attentional copulas.

## 5. Experiments

We start by evaluating the performance of TACTiS in comparison with state-of-the-art forecasting methods and then describe a series of additional experiments that assess other properties of TACTiS, such as the quality of the learned copula approximation and the model’s flexibility.

**Baselines** We benchmark against multiple deep-learning-based methods that generate multivariate probabilistic forecasts. These include GPVar (Salinas et al., 2019), an LSTM-based method that parametrizes a Gaussian copula, TempFlow (Rasul et al., 2021b) a transformer-based method that uses normalizing flows to model the predictive distribution, and TimeGrad (Rasul et al., 2021a) an autoregressive method that relies on diffusion models to estimate the predictive distribution.<sup>9</sup> We also include a comparison to classical methods: ARIMA (Box et al., 2015) and ETS exponential smoothing (Hyndman et al., 2008), as implemented in the R forecast package (Hyndman et al., 2022). These methods are compared against TACTiS-TT, a version of TACTiS that uses the temporal transformer layers of Tashiro et al. (2021), and TACTiS-GC, an ablation of our model that replaces the attentional copula of TACTiS-TT with the Gaussian copula of Salinas et al. (2019).

**Datasets** All methods are evaluated on four real-world datasets extracted from the *Monash Time Series Forecasting Repository* (Godahewa et al., 2021): electricity, solar-10min, fred-md, and kdd-cup. These datasets were selected due to being high-dimensional (107 to 321 time series), exempt from missing values for benchmarking purposes, and having diverse sampling frequencies (10 minutes, hourly, and monthly). See §C.1 for additional details.

**Metrics** Following related work, we choose the CRPS-Sum as our primary metric, which we use to compare forecasting methods and select their hyperparameters. This metric is calculated by taking the sum of the forecasted values for each series and applying the Continuous Ranked Probability Score (CRPS) (Matheson & Winkler, 1976) on said sum. The resulting metric can account for correlations between values of a given series but ignores correlations across series. Hence, we also evaluate the methods based on the energy score (Gneiting & Raftery, 2007), which is more expensive to compute but can capture correlations both within and across series. Both the CRPS and the energy score are detailed in §C.7.

**Evaluation procedure** Model accuracy is assessed through a backtesting procedure, which is detailed in §C.5, along with the hyperparameter selection protocol (§C.4). In short, we

<sup>9</sup>We also evaluated our method in comparison to CSDI (Tashiro et al., 2021), but have chosen to exclude these results at the moment due to the surprisingly poor performance of this baseline.

define a series of retraining timestamps for each dataset. At each timestamp, the models are trained with all of the preceding data, and their accuracy is assessed using subsequent data. This deviates from most related work, which often evaluates the models on a single training/testing split. However, the resulting evaluation is likely to be more faithful to the accuracy of these models when deployed in the real world.

**Benchmark results** The CRPS-Sum results for all models and datasets are shown in Tab. 1. From these, it is clear that TACTiS-TT compares favorably to the state of the art.

TACTiS-TT significantly outperforms all baselines on the electricity dataset, achieving a CRPS-Sum 40% lower than the second-best method. This difference is large considering that a CRPS-Sum of zero can only be reached by point forecasts with perfect foresight, which is obviously impossible in most situations. TACTiS-TT consistently ranks among the top three best-performing methods and its score is always within 25% of the best model. In contrast, all other baselines differ by at least 75% from the best score on one dataset.

The TACTiS-GC ablation of our model performs comparably to TACTiS-TT on most datasets. This may stem from a Gaussian copula being sufficient to capture the dependencies in the data. However, there are clear examples, such as the electricity dataset, where the additional flexibility of the attentional copula leads to much better performance.

Given these results, we conclude that TACTiS-TT ranks among the state of the art for this task. This is noteworthy given that it makes very few assumptions about the data distribution, compared to many of the baselines.

**Copula approximation quality** Theorem 4.1 states that our attentional copula will eventually converge to a true copula given unlimited capacity and training. However, it does not tell us how accurate this approximation is in practice. To assess the quality of the approximation, we measure how far the marginal distributions of attentional copulas are from  $U_{[0,1]}$  distributions. Such distances can be quantified using the Wasserstein distance (WD), a common metric for probability distributions.

We perform this evaluation using an instance of TACTiS-TT trained on the fred-md dataset<sup>10</sup> in the forecasting benchmark. We draw 1000 samples from its attentional copula (prior to applying the inverse CDF transform  $F_{\phi_k}^{-1}$ ) and compare these to an equally-sized sample from a  $U_{[0,1]}$ . This produces one WD value for each of the 1284 forecasted variables, resulting in the distribution<sup>11</sup> shown in Fig. 3 (mean 0.017). For reference, we also show the distribution of WD for a near-uniform distribution defined as  $\text{Beta}(1 + \varepsilon, 1 - \varepsilon)$ , where  $\varepsilon = 0.031$  is chosen to match the

<sup>10</sup>Selected for convenience due to its small size.

<sup>11</sup>The distribution is sensitive to sample size.

**Table 1:** CRPS-Sum means and standard deviations on backtesting benchmarks. Standard deviations are computed on both the various independent trials and the various backtesting timestamps (see §C.5). Best results are shown in bold.

Model	electricity	solar-10min	fred-md	kdd-cup
ETS	$0.059 \pm 0.032$	$0.678 \pm 0.269$	<b><math>0.037 \pm 0.032</math></b>	$0.408 \pm 0.068$
Auto-ARIMA	$0.077 \pm 0.052$	$0.994 \pm 0.623$	$0.043 \pm 0.019$	$0.625 \pm 0.326$
TempFlow	$0.072 \pm 0.081$	$0.565 \pm 0.151$	$0.095 \pm 0.012$	$0.260 \pm 0.036$
TimeGrad	$0.067 \pm 0.098$	$0.540 \pm 0.200$	$0.094 \pm 0.193$	$0.326 \pm 0.143$
GPVar	$0.035 \pm 0.036$	<b><math>0.254 \pm 0.088</math></b>	$0.067 \pm 0.028$	$0.290 \pm 0.027$
TACTiS-GC	$0.054 \pm 0.038$	$0.283 \pm 0.076$	$0.050 \pm 0.035$	<b><math>0.214 \pm 0.025</math></b>
TACTiS-TT	<b><math>0.021 \pm 0.016</math></b>	$0.314 \pm 0.183$	$0.040 \pm 0.025$	$0.253 \pm 0.055$

**Table 2:** Means of CRPS-Sum and energy scores for various bagging sizes (TACTiS-TT; data: fred-md).

Bag size ( $b$ )	CRPS-Sum	Energy score
1	0.051	$9.6 \times 10^5$
2	0.042	$8.3 \times 10^5$
5	0.042	$8.3 \times 10^5$
10	0.044	$8.8 \times 10^5$
15	0.040	$8.3 \times 10^5$
20	0.040	$8.4 \times 10^5$
30	0.042	$8.7 \times 10^5$

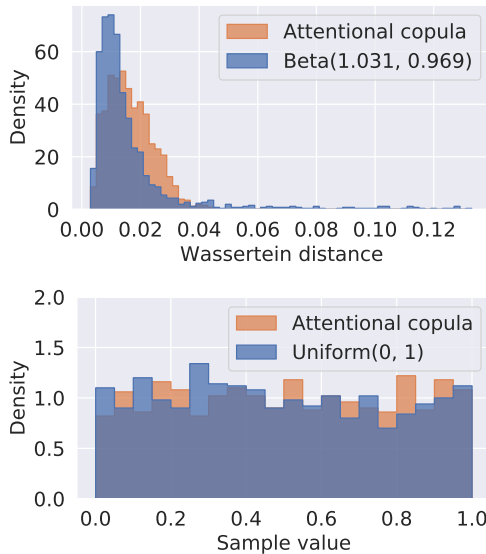


**Figure 3:** The marginal distributions of our attentional copulas resemble  $U_{[0,1]}$ . **(Top)** The copula marginal distributions tend to be similarly close to  $U_{[0,1]}$  than a near-uniform Beta distribution, according to the Wasserstein distance. **(Bottom)** The empirical density function of  $U_{[0,1]}$  and a representative marginal distribution from the copula are highly similar.

average WD of the attentional copula. Furthermore, Fig. 3 shows the distribution of attentional copula samples for a single variable, chosen to have WD the closest to the mean, and 1000 samples from a  $U_{[0,1]}$ . The resulting distributions are close. Together, these results show that the attentional copulas learned by TACTiS-TT can be good approximations of valid copulas, even in practical settings.

**Scalable training via subsampling** One key property of attention-based models, such as TACTiS, is that they can seamlessly be applied to settings of varying dimensionality, without retraining. We make use of this property to devise a scalable training procedure for TACTiS and its variants, which we detail in §B.3. In short, we train the model using batches composed of a random subset of  $b \ll n$  time series, called a *bag* ( $b = 20$  in the benchmark). This

significantly limits the running time and memory usage of the model. Then, at inference time only, we apply the model to all the series. In Tab. 2, we explore the effect of  $b$  on the CRPS-Sum and energy score metrics for the fred-md dataset. This parameter has very little impact on the accuracy of TACTiS-TT, with the exception of  $b = 1$ , which worsens results. This is to be expected since it prevents the model from learning dependencies between the series. This provides evidence that TACTiS-TT’s good performance is not only explained by good univariate forecasting, but also by properly learning dependencies between the series.

**Interpolation** In addition to its state-of-the-art forecasting performance, we demonstrate that TACTiS can achieve accurate probabilistic interpolation, i.e., predicting missing values within a time series. These results are reported in §D.

## 6. Discussion

This work proposes TACTiS, a method for probabilistic time series inference that combines the flexibility of attention-based models with the density estimation capabilities of a new type of non-parametric copula, termed attentional copula. In addition to achieving state-of-the-art performance on tasks such as probabilistic forecasting and interpolation, we showed that TACTiS reaches an unprecedented level of flexibility: it can infer missing values at arbitrary time points in multivariate time series (via masking), can handle the presence of observed non-stochastic covariates, can be trained even when subsets of the data are missing at random, and can estimate complex distributions beyond the reach of classical copula models, such as the Gaussian copula.

Despite this flexibility, there are several paths to extending TACTiS. First, while the model is technically compatible with unaligned and unevenly sampled time series, achieving good performance in these settings would likely require positional encodings that are more adapted to temporal data than those of Vaswani et al. (2017). Second, being based on transformers, TACTiS is resource hungry. While bagging allows training from hundreds of time series, it may be beneficial to apply recent advances in large-scale transformers (e.g.,

Choromanski et al. (2021)) to TACTiS. Third, TACTiS could be extended to series measured in discrete domains by adapting the estimation of marginal distributions in the decoder.

Finally, we believe that this work could serve as the basis for models that address the cold-start problem, making sensible predictions in contexts where very few (or no) historical observations of the process are available. In fact, TACTiS could be trained on time series from a wealth of domains, reusing the same attentional copula, but fine-tuning its encoder to new, unforeseen domains. These extensions towards a *foundation model* (Bommasani et al., 2021) for probabilistic time series inference are exciting future prospects.

## References

Aas, K., Czado, C., Frigessi, A., and Bakken, H. Pair-copula constructions of multiple dependence. *Insurance: Mathematics and Economics*, 44(2):182–198, 2009. URL <https://EconPapers.repec.org/RePEc:eee:insuma:v:44:y:2009:i:2:p:182-198>.

Alexandrov, A., Benidis, K., Bohlke-Schneider, M., Flunkert, V., Gasthaus, J., Januschowski, T., Maddix, D. C., Rangapuram, S., Salinas, D., Schulz, J., Stella, L., Türkmen, A. C., and Wang, Y. GluonTS: Probabilistic and Neural Time Series Modeling in Python. *Journal of Machine Learning Research*, 21(116):1–6, 2020. URL <http://jmlr.org/papers/v21/19-820.html>.

Bahdanau, D., Cho, K., and Bengio, Y. Neural machine translation by jointly learning to align and translate. In Bengio, Y. and LeCun, Y. (eds.), *3rd International Conference on Learning Representations, ICLR 2015, San Diego, CA, USA, May 7-9, 2015, Conference Track Proceedings*, 2015. URL <http://arxiv.org/abs/1409.0473>.

Benidis, K., Rangapuram, S. S., Flunkert, V., Wang, B., Maddix, D., Türkmen, C., Gasthaus, J., Bohlke-Schneider, M., Salinas, D., Stella, L., Callot, L., and Januschowski, T. Neural forecasting: Introduction and literature overview. *arXiv.org*, 2020. URL <http://arxiv.org/abs/2004.10240>.

Bohlke-Schneider, M. and Salinas, D. personal communication, 2021.

Bommasani, R., Hudson, D. A., Adeli, E., Altman, R., Arora, S., von Arx, S., Bernstein, M. S., Bohg, J., Bosselut, A., Bruskin, E., et al. On the opportunities and risks of foundation models. *arXiv preprint arXiv:2108.07258*, 2021.

Box, G. E. P., Jenkins, G. M., Reinsel, G. C., and Ljung, G. M. *Time series analysis: forecasting and control*. John Wiley & Sons, fifth edition, 2015.

Chapados, N. and Bengio, Y. Augmented functional time series representation and forecasting with gaussian processes. In Platt, J., Koller, D., Singer, Y., and Roweis, S. (eds.), *Advances in Neural Information Processing Systems*, volume 20. Curran Associates, Inc., 2007. URL <https://proceedings.neurips.cc/paper/2007/file/81e74d678581a3bb7a720b019f4f1a93-Paper.pdf>.

Chen, Y., Kang, Y., Chen, Y., and Wang, Z. Probabilistic forecasting with temporal convolutional neural network. *Neurocomputing*, 399:491–501, 2020.

Choromanski, K. M., Likhoshesterov, V., Dohan, D., Song, X., Gane, A., Sarlos, T., Hawkins, P., Davis, J. Q., Mohiuddin, A., Kaiser, L., Belanger, D. B., Colwell, L. J., and Weller, A. Rethinking attention with performers. In *International Conference on Learning Representations*, 2021. URL <https://openreview.net/forum?id=Ua6zuk0WRH>.

de Bézenac, E., Rangapuram, S. S., Benidis, K., Bohlke-Schneider, M., Kurle, R., Stella, L., Hasson, H., Gallinari, P., and Januschowski, T. Normalizing kalman filters for multivariate time series analysis. In Larochelle, H., Ranzato, M., Hadsell, R., Balcan, M. F., and Lin, H. (eds.), *Advances in Neural Information Processing Systems*, volume 33, pp. 2995–3007. Curran Associates, Inc., 2020. URL <https://proceedings.neurips.cc/paper/2020/file/1f47cef5e38c952f94c5d61726027439-Paper.pdf>.

Gneiting, T. and Raftery, A. E. Strictly proper scoring rules, prediction, and estimation. *Journal of the American statistical Association*, 102(477):359–378, 2007.

Godahewa, R., Bergmeir, C., Webb, G. I., Hyndman, R. J., and Montero-Manso, P. Monash time series forecasting archive. In *Neural Information Processing Systems Track on Datasets and Benchmarks*, 2021. forthcoming.

Goodfellow, I., Bengio, Y., and Courville, A. *Deep Learning*. MIT Press, 2016. <http://www.deeplearningbook.org>.

Größer, J. and Okhrin, O. Copulae: An overview and recent developments. *WIREs Computational Statistics*, n/a(n/a):e1557, 2021. doi: <https://doi.org/10.1002/wics.1557>. URL <https://wires.onlinelibrary.wiley.com/doi/abs/10.1002/wics.1557>. A good initial read to give a higher level of understanding of what copulas are and what kinds of copulas have been studied.

Ho, J., Jain, A., and Abbeel, P. Denoising diffusion probabilistic models. In Larochelle, H., Ranzato, M., Hadsell, R., Balcan, M. F., and Lin, H. (eds.), *Advances in Neural Information Processing Systems*, volume 33, pp. 6840–6851. Curran Associates, Inc., 2020. URL <https://proceedings.neurips.cc/paper/2020/file/4c5bcfec8584af0d967f1ab10179ca4b-Paper.pdf>.

Hochreiter, S. and Schmidhuber, J. Long short-term memory. *Neural computation*, 9(8):1735–1780, 1997.

Huang, C.-W., Krueger, D., Lacoste, A., and Courville, A. Neural autoregressive flows. In Dy, J. and Krause, A. (eds.), *Proceedings of the 35th International Conference on Machine Learning*, volume 80 of *Proceedings of Machine Learning Research*, pp. 2078–2087. PMLR, 10–15 Jul 2018. URL <https://proceedings.mlr.press/v80/huang18d.html>.

Hyndman, R., Koehler, A. B., Ord, J. K., and Snyder, R. D. *Forecasting with exponential smoothing: the state space approach*. Springer Science & Business Media, 2008.

Hyndman, R., Athanasopoulos, G., Bergmeir, C., Caceres, G., Chhay, L., O’Hara-Wild, M., Petropoulos, F., Razbash, S., Wang, E., and Yasmeen, F. *forecast: Forecasting functions for time series and linear models*, 2022. URL <https://pkg.robjhyndman.com/forecast/>. R package version 8.16.

Hyndman, R. J. and Khandakar, Y. Automatic time series forecasting: the forecast package for R. *Journal of Statistical Software*, 26(3):1–22, 2008. doi: 10.18637/jss.v027.i03.

Kim, S., Shephard, N., and Chib, S. Stochastic volatility: Likelihood inference and comparison with ARCH models. *The Review of Economic Studies*, 65(3):361–393, 07 1998. ISSN 0034-6527. URL <https://doi.org/10.1111/1467-937X.00050>.

Krupskii, P. and Joe, H. Flexible copula models with dynamic dependence and application to financial data. *Econometrics and Statistics*, 16:148–167, 2020. ISSN 2452-3062. doi: <https://doi.org/10.1016/j.ecosta.2020.01.005>. URL <https://www.sciencedirect.com/science/article/pii/S2452306220300216>.

Le Guen, V. and Thome, N. Probabilistic time series forecasting with shape and temporal diversity. In Larochelle, H., Ranzato, M., Hadsell, R., Balcan, M. F., and Lin, H. (eds.), *Advances in Neural Information Processing Systems*, volume 33, pp. 4427–4440. Curran Associates, Inc., 2020. URL <https://proceedings.neurips.cc/paper/2020/file/2f2b265625d76a6704b08093c652fd79-Paper.pdf>.

Li, S., Jin, X., Xuan, Y., Zhou, X., Chen, W., Wang, Y.-X., and Yan, X. Enhancing the locality and breaking the memory bottleneck of transformer on time series forecasting. In Wallach, H., Larochelle, H., Beygelzimer, A., d’Alché-Buc, F., Fox, E., and Garnett, R. (eds.), *Advances in Neural Information Processing Systems*, volume 32. Curran Associates, Inc., 2019. URL <https://proceedings.neurips.cc/paper/2019/file/6775a0635c302542da2c32aa19d86be0-Paper.pdf>.

Lim, B. and Zohren, S. Time-series forecasting with deep learning: a survey. *Philosophical Transactions of the Royal Society A: Mathematical, Physical and Engineering Sciences*, 379(2194):20200209, 2021. doi: 10.1098/rsta.2020.0209. URL <https://royalsocietypublishing.org/doi/abs/10.1098/rsta.2020.0209>.

Lim, B., Arik, S. Ö., Loeff, N., and Pfister, T. Temporal Fusion Transformers for interpretable multi-horizon time series forecasting. *International Journal of Forecasting*, 37(4):1748–1764, 2021. ISSN 0169-2070. doi: <https://doi.org/10.1016/j.ijforecast.2021.03.012>. URL <https://www.sciencedirect.com/science/article/pii/S0169207021000637>.

Lin, T., Wang, Y., Liu, X., and Qiu, X. A survey of transformers, 2021. URL <https://arxiv.org/abs/2106.04554>.

Lopez-Paz, D., Hernández-lobato, J., and Schölkopf, B. Semi-supervised domain adaptation with non-parametric copulas. In Pereira, F., Burges, C. J. C., Bottou, L., and Weinberger, K. Q. (eds.), *Advances in Neural Information Processing Systems*, volume 25. Curran Associates, Inc., 2012. URL <https://proceedings.neurips.cc/paper/2012/file/8e98d81f8217304975ccb23337bb5761-Paper.pdf>.

Makridakis, S., Spiliotis, E., and Assimakopoulos, V. Statistical and machine learning forecasting methods: Concerns and ways forward. *PLoS ONE*, 13(3):e0194889–26, 2018.

Makridakis, S., Spiliotis, E., Assimakopoulos, V., Chen, Z., Gaba, A., Tsetlin, I., and Winkler, R. L. The M5 uncertainty competition: Results, findings and conclusions. *International Journal of Forecasting*, 2021. ISSN 0169-2070. doi: <https://doi.org/10.1016/j.ijforecast.2021.10.009>. URL <https://www.sciencedirect.com/science/article/pii/S0169207021001722>.

Makridakis, S., Spiliotis, E., and Assimakopoulos, V. M5 accuracy competition: Results, findings, and conclusions. *International Journal of Forecasting*, 2022. ISSN 0169-2070. doi: <https://doi.org/10.1016/j.ijforecast.2021.11.013>. URL <https://www.sciencedirect.com/science/article/pii/S0169207021001874>.

Matheson, J. E. and Winkler, R. L. Scoring rules for continuous probability distributions. *Management science*, 22(10):1087–1096, 1976.

Mayer, A. and Wied, D. Estimation and inference in factor copula models with exogenous covariates, 2021. URL <https://arxiv.org/abs/2107.03366>.

Montero-Manso, P. and Hyndman, R. J. Principles and algorithms for forecasting groups of time series: Locality and globality. *International Journal of Forecasting*, 37(4):1632–1653, 2021. ISSN 0169-2070. doi: <https://doi.org/10.1016/j.ijforecast.2021.03.004>. URL <https://www.sciencedirect.com/science/article/pii/S0169207021000558>.

Müller, S., Hollmann, N., Arango, S. P., Grabocka, J., and Hutter, F. Transformers can do Bayesian inference. In *International Conference on Learning Representations*, 2022. URL <https://openreview.net/forum?id=KSugKcbNf9>.

Nelsen, R. B. *An introduction to copulas*. Springer Science & Business Media, second edition, 2007.

Orshkin, B. N., Carpow, D., Chapados, N., and Bengio, Y. N-BEATS: Neural basis expansion analysis for interpretable time series forecasting. In *International Conference on Learning Representations*, 2020. URL <https://openreview.net/forum?id=r1ecqn4YwB>.

Papamakarios, G., Nalisnick, E., Rezende, D. J., Mohamed, S., and Lakshminarayanan, B. Normalizing flows for probabilistic modeling and inference. *Journal of Machine Learning Research*, 22(57):1–64, 2021. URL <http://jmlr.org/papers/v22/19-1028.html>.

Paszke, A., Gross, S., Massa, F., Lerer, A., Bradbury, J., Chanan, G., Killeen, T., Lin, Z., Gimelshein, N., Antiga, L., Desmaison, A., Kopf, A., Yang, E., DeVito, Z., Raison, M., Tejani, A., Chilamkurthy, S., Steiner, B., Fang, L., Bai, J., and Chintala, S. Pytorch: An imperative style, high-performance deep learning library. In Wallach, H., Larochelle, H., Beygelzimer, A., d’Alché Buc, F., Fox, E., and Garnett, R. (eds.), *Advances in Neural Information Processing Systems 32*, pp. 8024–8035. Curran Associates, Inc., 2019. URL <http://papers.neurips.cc/paper/9015-pytorch-an-imperative-style-high-performance-deep-learning-library.pdf>.

Patton, A. J. A review of copula models for economic time series. *Journal of Multivariate Analysis*, 110:4–18, 2012.

Peterson, M. *An Introduction to Decision Theory*. Cambridge Introductions to Philosophy. Cambridge University Press, second edition, 2017. doi: 10.1017/9781316585061.

R Core Team. *R: A Language and Environment for Statistical Computing*. R Foundation for Statistical Computing, Vienna, Austria, 2020. URL <https://www.R-project.org/>.

Rasul, K. PyTorchTS, 2021a. URL <https://github.com/zalandoresearch/pytorch-ts>.

Rasul, K. personal communication, 2021b.

Rasul, K., Seward, C., Schuster, I., and Vollgraf, R. Autoregressive denoising diffusion models for multivariate probabilistic time series forecasting. In Meila, M. and Zhang, T. (eds.), *Proceedings of the 38th International Conference on Machine Learning*, volume 139 of *Proceedings of Machine Learning Research*, pp. 8857–8868. PMLR, 18–24 Jul 2021a. URL <https://proceedings.mlr.press/v139/rasul21a.html>.

Rasul, K., Sheikh, A.-S., Schuster, I., Bergmann, U. M., and Vollgraf, R. Multivariate probabilistic time series forecasting via conditioned normalizing flows. In *International Conference on Learning Representations*, 2021b. URL <https://openreview.net/forum?id=WiGQBFuVRv>.

Rémillard, B., Papageorgiou, N., and Soustra, F. Copula-based semiparametric models for multivariate time series. *Journal of Multivariate Analysis*, 110:30–42, 2012. ISSN 0047-259X. doi: <https://doi.org/10.1016/j.jmva.2012.03.001>. URL <https://www.sciencedirect.com/science/article/pii/S0047259X1200070X>. Special Issue on Copula Modeling and Dependence.

Salinas, D., Bohlke-Schneider, M., Callot, L., Medico, R., and Gasthaus, J. High-dimensional multivariate forecasting with low-rank Gaussian copula processes. *Advances in Neural Information Processing Systems*, 32: 6827–6837, 2019.

Salinas, D., Flunkert, V., Gasthaus, J., and Januschowski, T. DeepAR: Probabilistic forecasting with autoregressive recurrent networks. *International Journal of Forecasting*, 36(3):1181–1191, 2020.

Seabold, S. and Perktold, J. statsmodels: Econometric and statistical modeling with Python. In *9th Python in Science Conference*, 2010.

Shih, S.-Y., Sun, F.-K., and Lee, H.-y. Temporal pattern attention for multivariate time series forecasting. *Machine Learning*, 108(8-9):1421–1441, 2019.

Shukla, S. N. and Marlin, B. Multi-time attention networks for irregularly sampled time series. In *International Conference on Learning Representations*, 2021a. URL [https://openreview.net/forum?id=4c0J61wQ4\\_](https://openreview.net/forum?id=4c0J61wQ4_).

Shukla, S. N. and Marlin, B. M. A survey on principles, models and methods for learning from irregularly sampled time series, 2021b. URL <https://arxiv.org/abs/2012.00168>.

Sklar, A. Fonctions de répartition à  $n$  dimensions et leurs marges. *Publications de l’Institut Statistique de l’Université de Paris*, 8:229–231, 1959.

Sohl-Dickstein, J., Weiss, E., Maheswaranathan, N., and Ganguli, S. Deep unsupervised learning using nonequilibrium thermodynamics. In Bach, F. and Blei, D. (eds.), *Proceedings of the 32nd International Conference on Machine Learning*, volume 37 of *Proceedings of Machine Learning Research*, pp. 2256–2265, Lille, France, 07–09 Jul 2015. PMLR. URL <https://proceedings.mlr.press/v37/sohl-dickstein15.html>.

Spadon, G., Hong, S., Brandoli, B., Matwin, S., Rodrigues-Jr, J. F., and Sun, J. Pay attention to evolution: Time series forecasting with deep graph-evolution learning. *IEEE Transactions on Pattern Analysis & Machine Intelligence*, 2021. ISSN 1939-3539. doi: 10.1109/TPAMI.2021.3076155.

Stan Development Team. Stan modeling language users guide and reference manual, 2022. URL <https://mc-stan.org>.

Sun, C., Hong, S., Song, M., and Li, H. A review of deep learning methods for irregularly sampled medical time series data, 2020. URL <https://arxiv.org/abs/2010.12493>.

Tabak, E. G. and Turner, C. V. A family of nonparametric density estimation algorithms. *Communications on Pure and Applied Mathematics*, 66(2):145–164, 2013.

Tang, B. and Matteson, D. Probabilistic transformer for time series analysis. *Advances in Neural Information Processing Systems*, 34, 2021.

Tashiro, Y., Song, J., Song, Y., and Ermon, S. CSDI: Conditional score-based diffusion models for probabilistic time series imputation. In *Advances in Neural Information Processing Systems*, volume 34, 2021.

Tay, Y., Dehghani, M., Bahri, D., and Metzler, D. Efficient transformers: A survey, 2020. URL <https://arxiv.org/abs/2009.06732>.

van den Oord, A., Dieleman, S., Zen, H., Simonyan, K., Vinyals, O., Graves, A., Kalchbrenner, N., Senior, A., and Kavukcuoglu, K. Wavenet: A generative model for raw audio. In *Arxiv*, 2016. URL <https://arxiv.org/abs/1609.03499>.

Vaswani, A., Shazeer, N., Parmar, N., Uszkoreit, J., Jones, L., Gomez, A. N., Kaiser, Ł., and Polosukhin, I. Attention is all you need. In *Advances in neural information processing systems*, pp. 5998–6008, 2017.

Wei, W. W. *Multivariate time series analysis and applications*. John Wiley & Sons, 2018.

Williams, C. K. and Rasmussen, C. E. *Gaussian processes for machine learning*, volume 2. MIT press Cambridge, MA, 2006.

Yanchenko, A. K. and Mukherjee, S. Stanza: A nonlinear state space model for probabilistic inference in non-stationary time series. *arXiv*, pp. 2006.06553v1, 2020.

Zhang, G., Eddy Patuwo, B., and Y. Hu, M. Forecasting with artificial neural networks:: The state of the art. *International Journal of Forecasting*, 14(1):35–62, 1998. ISSN 0169-2070. doi: [https://doi.org/10.1016/S0169-2070\(97\)00044-7](https://doi.org/10.1016/S0169-2070(97)00044-7). URL <https://www.sciencedirect.com/science/article/pii/S0169207097000447>.

## A. Proof of Theorem 4.1

**Theorem 4.1.** The copula  $c_{\phi_c^\pi}$  embedded in a density estimator  $g_{\phi^\pi}$ , as shown in Eq. (5), with distributional parameters  $\phi^\pi$  given by a decoder with parameters by  $\theta_{\text{dec}} \in \Theta$ , where  $\Theta$  minimizes Eq. (10), is a valid copula.

*Proof.* To show that  $c_{\phi_c^\pi}(u_1^{(m)}, \dots, u_{n_m}^{(m)})$  is the density of a valid copula, we need to show two properties: 1) it is a distribution on the unit cube  $[0, 1]^{n_m}$ , 2) the marginal distribution of each random variable is uniform.

*Property (1)* is trivially satisfied since, by construction, the support of each conditional distribution is limited to the  $[0, 1]$  interval (see §4.2, paragraph *Choice of distribution*).

*Property (2)* is a consequence of minimizing the problem in Eq. (10). Recall that the parameters of the decoder,  $\theta_{\text{dec}}$ , are obtained by minimizing the following expression:

$$\begin{aligned} \mathbb{E}_{\substack{\pi \sim \Pi \\ \mathbf{x} \sim \mathcal{S}}} - \log g_{\phi^\pi}(x_1^{(m)}, \dots, x_{n_m}^{(m)}) &= \mathbb{E}_{\mathbf{x} \sim \mathcal{S}} - \frac{1}{|\Pi|} \sum_{\pi \in \Pi} \log g_{\phi^\pi}(x_1^{(m)}, \dots, x_{n_m}^{(m)}) \\ &= \mathbb{E}_{\mathbf{x} \sim \mathcal{S}} - \frac{1}{|\Pi|} \log \left[ \prod_{\pi \in \Pi} g_{\phi^\pi}(x_1^{(m)}, \dots, x_{n_m}^{(m)}) \right] \\ &= \mathbb{E}_{\mathbf{x} \sim \mathcal{S}} - \log \left[ \prod_{\pi \in \Pi} g_{\phi^\pi}(x_1^{(m)}, \dots, x_{n_m}^{(m)}) \right]^{|\Pi|^{-1}}. \end{aligned} \quad (11)$$

Notice that the term inside of the logarithm in Eq. (11) corresponds to a geometric mean. This quantity is always smaller or equal to the arithmetic mean and equality is reached i.i.f. all elements over which the mean is calculated are equal. Hence, we can rewrite the expression in Eq. (11) as:

$$\mathbb{E}_{\mathbf{x} \sim \mathcal{S}} - \log \left[ \frac{1}{|\Pi|} \sum_{\pi \in \Pi} g_{\phi^\pi}(x_1^{(m)}, \dots, x_{n_m}^{(m)}) \right] + \delta,$$

where  $\delta \in \mathbb{R}^+$  is exactly zero i.i.f. the density estimated by the model is permutation invariant, i.e.,  $g_{\phi^\pi}(x_1^{(m)}, \dots, x_{n_m}^{(m)}) = g_\phi(x_1^{(m)}, \dots, x_{n_m}^{(m)})$ ,  $\forall \pi \in \Pi$ .

Based on this expression, we conclude that the parameters  $\theta_{\text{dec}}$  that minimize the problem in Eq. (10) lead a density estimator that (i) is invariant to permutations  $\pi$  and (ii) that minimizes the negative log-likelihood of the data  $\mathbb{E}_{\mathbf{x} \sim \mathcal{S}} - \log g_\phi(x_1^{(m)}, \dots, x_{n_m}^{(m)})$ . It naturally follows from Eq. (5) that the embedded copula density  $c_{\phi_c^\pi}(u_1^{(m)}, \dots, u_{n_m}^{(m)})$  is also permutation invariant.

Now, recall that, by construction, the marginal density of the first element in a permutation  $c_{\phi_{c1}^\pi}(u_1)$ , is taken to be that of a  $U_{[0,1]}$  (see §4.2, paragraph *Copula density*). Given that the copula density  $c_{\phi_{c1}^\pi}(u_1^{(m)}, \dots, u_{n_m}^{(m)})$  is invariant to permutations, the marginal distribution of all variables must necessarily be  $U_{[0,1]}$ . Thus, *Property (2)* is satisfied.

Since *Properties (1) and (2)* are both satisfied, we conclude that the attentional copula  $c_{\phi_c^\pi}$ , with parameters obtained from a decoder with parameters  $\theta_{\text{enc}}$  is a valid copula.

□

## B. Implementation details

### B.1. Libraries used

We have implemented TACTiS-TT and TACTiS-GC using the PyTorchTS library (Rasul, 2021a) and PyTorch (Paszke et al., 2019). The PyTorchTS library allows models using PyTorch to interact with the GluonTS library (Alexandrov et al., 2020), which we have used to handle the datasets and our experiments. Our implementation will be made available upon acceptance.

## B.2. Inverting the flow

When sampling, we need to compute the inverses of the marginal distributions of the sampled variables:  $F_{\phi_k}^{-1}(u_k^{(m)})$ . Since  $F_{\phi_k}(x_k^{(m)})$  is strictly monotonic by construction, many search algorithms can be applied here. Due to its high numerical stability and ease of implementation, we elected to use a binary search here. While the binary search is relatively slow, this is barely relevant when compared to the rest of the decoder, mainly the transformer layers in the copula.

## B.3. Bagging

Three of the models in our benchmarks, namely GPVar, TACTiS-GC, and TACTiS-TT, can be trained with any subset of the series from the dataset, without having to adjust their parameters. This allows us to severely reduce the number of series sent to the model at once during training time, thus greatly reducing the model memory footprint. For both models, we randomly select 20 series for each data sample sent to the model during training. For sampling, all series are sent to the model.

As mentioned in §C.2, we increase the number of samples sent per epochs to these models to compensate for the reduced amount of data per sample due to the bagging procedure.

## B.4. Data normalization

It is often desirable for a model to be scale and translation invariant. For TACTiS-TT, we thus transform the data according to what we call the "Standardization" procedure. For each sample, we compute the means and variances for each series using only the values of the observed tokens  $\{x_{ij}^{(o)}\}$ . The values of both the observed and missing tokens is then transformed using

$$\tilde{x}_{ij} = \frac{x_{ij} - \text{mean}_i}{\sqrt{\text{variance}_i}}. \quad (12)$$

After sampling, we can undo this transformation using

$$x_{ij} = \sqrt{\text{variance}_i} \times \tilde{x}_{ij} + \text{mean}_i. \quad (13)$$

Note that if all values are identical for a given series, we replace the variance by 1 to avoid divisions by zero.

## C. Forecasting Benchmark Experimental setup

### C.1. Choice of datasets for the benchmarks

**Table 3:** Dimensions and prediction lengths of the datasets used in our benchmarks, along with the short name by which they are referred as in this paper.

Short name	Monash name	Frequency	Number of series	Prediction length
electricity	Electricity Hourly Dataset	1 hour	321	24
solar-10min	Solar Dataset (10 Minutes Observations)	10 minutes	137	72
fred-md	FRED-MD Dataset	1 month	107	12
kdd-cup	KDD Cup Dataset (without Missing Values)	1 hour	270	48

Table 3 describes the four datasets that have been selected for our benchmarks. These datasets have been selected due to being publicly available at the Monash Time Series Forecasting Repository (Godahewa et al., 2021), not having any missing values, and having a large enough number of series without being too high for transformer-based models. A modified version of the electricity dataset is often used in the benchmarks of other models, allowing us to compare our results with the model creator's results, thus giving us confidence in our own. The hourly-frequency version of the solar-10min is also often used, although we opted for the 10 minutes frequency version to have another frequency. It was restricted to a prediction length of 72 (12 hours) due to a prediction length of 144 (24 hours) being too taxing for the transformer-based models. The fred-md dataset was selected due to its series being various economic indicators, thus showing a wide variety of behaviors. Finally, the kdd-cup dataset was given a prediction length of 48 (2 days) to give a different challenge to the models than the electricity dataset.

Each dataset was downloaded from the Monash Repository using GluonTS (Alexandrov et al., 2020). The only modification to the data is the rescaling that some of the models require.

## C.2. Training procedure for deep learning models

For the deep learning models in our benchmarks (TempFlow, TimeGrad, GPVar, and TACTis-TT) we used the same training procedure, with a few exceptions for GPVar described in §C.2.1. Each training is done in a Docker container giving access to an NVIDIA Tesla P100 GPU with 12 GB of GPU RAM, 2 CPU cores, and 32 GB of CPU RAM.

Since the models are quite memory-intensive, and the amount needed can vary quite a bit based on the hyperparameters and which dataset is being used, we could not select batch sizes directly. To select the batch sizes, we ran a small number of training iterations at various batch sizes (powers of two from 1 to 256) and kept the highest one which did not result in an out-of-memory error. While this method is crude, it allows hyperparameters that use less memory to take advantage of the available memory to be faster through higher parallelization.

In each training epoch, the model will see the data from 1600 samples from the training set. Since the batch size is variable, we thus do  $\lfloor 1600/\text{batch size} \rfloor$  iterations per epoch. As is explained in §B.3, the GPVar, TACTis-GC, and TACTis-TT models use bagging during training, and thus only see a random subset of all series at each iteration. To compensate for this, the number of iterations for these models is increased to  $\lfloor (1600/\text{batch size}) \times (\text{number of series}/\text{bagging size}) \rfloor$ . The batches are built by randomly picking windows of length equal to the sum of the prediction and history lengths in the training dataset. Only complete windows are considered, and they all have equal probability to be selected.

After each epoch, we compute a validation loss on the training set. The training ends when the first of the following condition is reached:

- The model has trained for 200 epochs,
- The model has trained for more than 3 days, or
- It has been 20 epochs since the best validation loss.

The resulting model which is used to compute the metrics is the one that minimized the validation loss, and not necessarily the one at the last epoch.

### C.2.1. GPVAR

Following communication with GPVar authors (Bohlke-Schneider & Salinas, 2021), we trained that model on CPU instead of GPU, due to performance concerns. To compensate for not having a GPU, we allocate 8 cores and 64 GB of RAM instead of the 2 and 32 respectively for the models trained using a GPU. Furthermore, we use the GluonTS Trainer for GPVar, and thus use its own training ending conditions, with an additional maximum time at 3 days.

## C.3. Classical models

Our Auto-ARIMA results are obtained by running the `auto.arima` function (Hyndman & Khandakar, 2008) of the `forecast` package (Hyndman et al., 2022) in the R programming language (R Core Team, 2020). This performs an automatic search of the model specification on a per-time series basis. Since the function supports univariate time series only, we run the function independently for each time series (i.e. we treat a  $d$ -dimensional multivariate problem as  $d$  independent univariate problems), with both the hyperparameters and parameters being specific to each time series. We restrict the search to SARIMA models with maximum order  $p = 3, q = 3, P = 2, Q = 2$ , and the default values for the other function parameters. We carry out an automatic Box-Cox transformation for positive-valued time series. For each time series, we limit fitting time to a maximum of 30 minutes, reverting to a simpler ARMA(1, 1) model with no seasonality or Box-Cox transformation if the original fitting fails. A fit is considered to have failed if the following conditions are encountered:

- Maximum time limit is exceeded;
- The in-sample fitted values contain non-finite values;
- Fewer than 20% of the simulated predictive trajectories contain finite values (e.g. the predictive simulations diverge), or contain values that are not within a factor 1,000 (in absolute value) of the training observations.

Our ETS (error, trend, seasonality) exponential smoothing (Hyndman et al., 2008) results are obtained through the `ETSModel` implementation within Python's `statsmodels` package (Seabold & Perktold, 2010). This implementation replicates the R implementation within the `forecast` package discussed above. An automatic hyperparameter search is carried out to select, on a *per-dataset basis*, the following hyperparameters:

- Trend: either none or additive;

- Seasonality: either none or additive.

For robustness across a wide variety of datasets, the error term is always considered additive. As with the ARIMA results, since ETS is univariate, independent fitting and predictive simulations of the model are carried out for each time series.

#### C.4. Hyperparameter search

For each model and each dataset under consideration, we do a hyperparameter search to find the best hyperparameters that will be used when comparing the forecasting quality of the models. We opted to do such a search instead of selecting the published parameters since not all of the selected datasets have been used in previously published articles, and to allow us to have a fair comparison by having equally-extensive searches for all models.

From each dataset, the final subset of the time steps is reserved for the backtesting procedure which will be described in §C.5. From the remaining time steps, a window at the end of length equals to 7 times the prediction length is reserved as the validation set, which is used to compute the metrics. All the data prior to the validation set is used as the training set during the hyperparameter search.

For each hyperparameter search, we try 50 sets of hyperparameters, randomly selected amongst the possible combinations for the model. For each set of hyperparameters, we train the model 5 times, using independent initial parameters and sampling orders. Forecasts are then obtained on each possible prediction window that fits inside the validation set. The CRPS-Sum is computed on 100 samples from each of these forecasts, and the values for the various prediction windows are averaged.

The best set of hyperparameters is then the one where none of the 5 trained models failed due to numerical or memory error, and for which the worst CRPS-Sum value amongst the 5 trained models is the lowest. The reason we are taking the worst of 5 instead of the mean or median is that we have observed that for some architectures (such as TACTiS-GC), some hyperparameters lead to unstable training, sometimes giving great results and sometimes giving awful results. We want to avoid selecting such hyperparameters since such instability would be unfit for real-world applications.

#### C.5. Backtesting

The main reason why we recomputed the metrics for competing models in our benchmarks is to use our backtesting framework. The backtesting framework’s goal is to simulate how such models would be used in practice. In practice, hyperparameter search is expensive, and so would only be done seldomly. Training the model is less expensive, but not cheap either, so would be redone periodically to allow the model to learn from newer behavior in the data. Finally, forecasting using an already trained model is cheap, and would be done as needed. Therefore, in our framework, we do a single hyperparameter search, multiple model training, and multiple forecasting per model training.

For each dataset, we define  $n_B$  backtesting timestamps  $\tau_1, \tau_2, \dots, \tau_{n_B}$ . For each backtesting timestamp  $\tau_i$ , we further define multiple forecasting timestamps  $\tau_{i1}, \tau_{i2}, \dots, \tau_{iN_F}$ . The hyperparameter search described in §C.4 is done using only data prior to  $\tau_1$ , while the  $i$ -th model is trained using only with the data prior to  $\tau_i$ .

We use  $n_B = 6$  for all datasets. For electricity, we select Mondays at midnight for the  $\tau_i$ , with one week between each, and do a forecast every 24 hours between them. For solar-10min, we also select Mondays at midnight for the  $\tau_i$ , with one week between each, and do a forecast every 12 hours between them. For fred-md, we select Januaries for the  $\tau_i$ , with one year between each, and do a single forecast on January. For kdd-cup, we also select Mondays at midnight for the  $\tau_i$ , with two weeks between each, and do a forecast every 48 hours between them. For each dataset, we select the last possible timestamps which followed these criteria and still had enough data for a full prediction range.

The training is done as explained in §C.2, except that we do not have validation sets for the early stopping procedure. Instead, we use the maximum number of epochs at which we reached the best validation loss during hyperparameter search for the winning hyperparameters.

#### C.6. Hyperparameter ranges

In this section, we list the possible values for the hyperparameters we used for the hyperparameter searches. These hyperparameters for the competing models are inspired by the hyperparameters used in their respective papers and implementations.

Tables 4 and 5 show the hyperparameters for the TACTiS-TT and TACTiS-GC models, respectively. The CDF normalization refer to transforming the data according to the empirical CDF computed from the history of each sample, followed by the

inverse CDF of normal distribution of zero mean and unit variance.

**Table 4:** Possible hyperparameters for TACTiS-TT.  $e$ ,  $s$ ,  $f$ , and  $k$  respectively indicate the optimal hyperparameters for electricity, solar-10min, fred-md, and kdd-cup.

	Hyperparameter	Possible values
Model	Encoder transformer embedding size (per head) and feed forward network size	$8^k, 16^f, 24^s$
	Encoder transformer number of heads	$1^{sfk}, 2^e, 3$
	Encoder number of transformer layers pairs	$1^s, 2^f, 3^k$
	Encoder time series embedding dimensions	$5^{esfk}$
	Decoder MLP number of layers	$1^{esk}, 2^f, 4$
	Decoder MLP hidden dimensions	$8^{ef}, 16, 24^{sk}$
	Decoder transformer number of heads	$1, 2, 3^{esfk}$
	Decoder transformer embedding size (per head)	$8^{esf}, 16^k, 24$
	Decoder number transformer layers	$1^{ef}, 2^s, 3^k$
	Decoder number of bins in conditional distribution	$20^{esf}, 50^k, 100$
	Decoder DSF number of layers	$2^{sfk}, 3^e$
	Decoder DSF hidden dimensions	$8^f, 16^{esk}$
	Dropout	$0^{sfk}, 0.1, 0.01^e$
	Normalization	Standardization $^{esfk}$
Training	History length to prediction length ratio	$1^k, 2^{sk}, 3^e$
	Optimizer	RMSprop $^{esfk}$
	Learning rate	$(10^{-4})^s, (10^{-3})^{efk}, (10^{-2})$
	Weight decay	$0^e, (10^{-5})^{sk}, (10^{-4})^f, (10^{-3})$
	Gradient clipping	$(10^3)^{esfk}, (10^4)$

**Table 5:** Possible hyperparameters for TACTiS-GC.  $e$ ,  $s$ ,  $f$ , and  $k$  respectively indicate the optimal hyperparameters for electricity, solar-10min, fred-md, and kdd-cup.

	Hyperparameter	Possible values
Model	Encoder transformer embedding size (per head) and feed forward network size	$8^f, 16^e, 24^{sk}$
	Encoder transformer number of heads	$1, 2^{esfk}$
	Encoder number of transformer layers pairs	$1^{ef}, 2, 4^{sk}$
	Encoder time series embedding dimensions	$5^{esfk}$
	Decoder MLP number of layers	$1^s, 2^k, 4^{ef}$
	Decoder MLP hidden dimensions and rank of the low-rank approximation	$8^e, 16^k, 24^{sf}$
	Dropout	$0^{es}, 0.1^f, 0.01^k$
	Normalization	None $^s$ , Standardization $^e$ , CDF $^{fk}$
	History length to prediction length ratio	$1^f, 2^e, 3^{sk}$
	Optimizer	RMSprop $^{esfk}$
	Learning rate	$(10^{-4})^s, (10^{-3})^{efk}, (10^{-2})$
	Weight decay	$0, (10^{-5})^{ef}, (10^{-4})^k, (10^{-3})^s$
	Gradient clipping	$(10^3)^{esfk}, (10^4)$

Table 6 shows the hyperparameters for the TempFlow model. Parameters in `teletype` font refer to parameters in the authors implementation in PyTorchTS (Rasul, 2021a), with all other parameters left at their default value. The choice of possible hyperparameters for the TempFlow model has been discussed with its authors (Rasul, 2021b).

Table 7 shows the hyperparameters for the TimeGrad model. Parameters in `teletype` font refer to parameters in the authors implementation in PyTorchTS (Rasul, 2021a), with all other parameters left at their default value.

Table 8 shows the hyperparameters for the GPVar model. Parameters in `teletype` font refer to parameters in the authors implementation in GluonTS (Alexandrov et al., 2020), with all other parameters left at their default value.

**Table 6:** Possible hyperparameters for TempFlow.  $\mathbf{e}$ ,  $\mathbf{s}$ ,  $\mathbf{f}$ , and  $\mathbf{k}$  respectively indicate the optimal hyperparameters for electricity, solar-10min, fred-md, and kdd-cup.

Hyperparameter		Possible values
Model	d_model	16, 32 $\mathbf{k}$ , 64 $\mathbf{es}$ , 128, 256 $\mathbf{f}$
	dim_feedforward_scale	1 $\mathbf{e}$ , 2, 4 $\mathbf{sfk}$
	num_heads	1 $\mathbf{f}$ , 2 $\mathbf{s}$ , 4, 8 $\mathbf{ek}$
	num_encoder_layers	1, 3 $\mathbf{k}$ , 5 $\mathbf{esf}$
	num_decoder_layers	1 $\mathbf{e}$ , 3 $\mathbf{f}$ , 5 $\mathbf{sk}$
	dropout_rate	0 $\mathbf{es}$ , 0.01 $\mathbf{k}$ , 0.1 $\mathbf{f}$
	flow_type	"RealNVP" $\mathbf{esk}$ , "MAF" $\mathbf{f}$
	n_blocks	1 $\mathbf{f}$ , 3, 5 $\mathbf{esk}$
	hidden_size	8, 16 $\mathbf{f}$ , 32 $\mathbf{s}$ , 64 $\mathbf{k}$ , 128 $\mathbf{e}$
	n_hidden	1, 2 $\mathbf{fk}$ , 4 $\mathbf{es}$
	conditioning_length	8, 16, 32, 64 $\mathbf{k}$ , 128 $\mathbf{e}$
	dequantize	False $\mathbf{esk}$ , True $\mathbf{f}$
Data	History length to prediction length ratio	1 $\mathbf{efk}$ , 2 $\mathbf{s}$ , 3
Training	Optimizer	Adam $\mathbf{esfk}$
	Learning rate	(10 $^{-4}$ ) $\mathbf{sf}$ , (10 $^{-3}$ ) $\mathbf{e}$ , (10 $^{-2}$ ) $\mathbf{k}$
	Gradient clipping	(10 $^1$ ) $\mathbf{sk}$ , (10 $^2$ ) $\mathbf{ef}$ , (10 $^4$ )

**Table 7:** Possible hyperparameters for TimeGrad.  $\mathbf{e}$ ,  $\mathbf{s}$ ,  $\mathbf{f}$ , and  $\mathbf{k}$  respectively indicate the optimal hyperparameters for electricity, solar-10min, fred-md, and kdd-cup.

Hyperparameter		Possible values
Model	num_layers	1 $\mathbf{e}$ , 2 $\mathbf{k}$ , 4 $\mathbf{sf}$
	num_cells	8, 16 $\mathbf{sf}$ , 24 $\mathbf{k}$ , 32, 40 $\mathbf{e}$
	cell_type	"lstm" $\mathbf{sfk}$ , "gru" $\mathbf{e}$
	use_marginal_transformation	True $\mathbf{esfk}$ , False
	rank	8 $\mathbf{f}$ , 16 $\mathbf{ek}$ , 24 $\mathbf{s}$
	dropout_rate	0 $\mathbf{f}$ , 0.01 $\mathbf{e}$ , 0.1 $\mathbf{sk}$
Data	History length to prediction length ratio	1, 2 $\mathbf{s}$ , 3 $\mathbf{efk}$
Training	Optimizer	Adam $\mathbf{esfk}$
	Learning rate	(10 $^{-4}$ ) $\mathbf{ef}$ , (10 $^{-3}$ ) $\mathbf{sk}$ , (10 $^{-2}$ )
	Weight decay	0 $\mathbf{k}$ , (10 $^{-8}$ ) $\mathbf{f}$ , (10 $^{-5}$ ), (10 $^{-4}$ ), (10 $^{-3}$ ) $\mathbf{es}$
	Gradient clipping	10 $\mathbf{esfk}$

## C.7. Metrics

As mentioned in §5, we use the CRPS-Sum as our primary metric, both to select the best hyperparameters, and to compare the forecasting accuracy of the various models. The CRPS-Sum is based on the Continuous Ranked Probability Score (CRPS) (Matheson & Winkler, 1976), which can be computed for each individual forecasted value for the  $i$ -th series and the  $j$ -th timestep as:

$$\text{CRPS}(X_{ij}, x_{ij}) = \mathbb{E}_{X_{ij}} [|X_{ij} - x_{ij}|] - \frac{1}{2} \mathbb{E}_{X_{ij}, X'_{ij}} [|X_{ij} - X'_{ij}|], \quad (14)$$

where  $x_{ij}$  is the observed value and  $X_{ij}$  and  $X'_{ij}$  are two independent variables from the forecasted sampling process. The CRPS-Sum is obtained by replacing the individual values by the sum over all timesteps:  $s_i = \sum_j x_{ij}$  and  $S_i = \sum_j X_{ij}$ , where the sum is over the timesteps where the forecast is made. This transformation of the CRPS-Sum allows it to capture the quality of some of the correlations in the forecasts: namely the average correlation between forecasts inside a single series. However, the CRPS-Sum metric is inherently univariate, and cannot discriminate whether the forecasting method accurately predicts the correlation between series or not.

**Table 8:** Possible hyperparameters for GPVar.  $^e$ ,  $^s$ ,  $^f$ , and  $^k$  respectively indicate the optimal hyperparameters for electricity, solar-10min, fred-md, and kdd-cup.

Hyperparameter		Possible values
Model	num_layers	1, 2, 3 $^{esfk}$
	num_cells	20 $^f$ , 40 $^s$ , 60 $^e$
	dropout_rate	0 $^f$ , 0.01 $^e$ , 0.1 $^k$
	diff_steps	25, 50, 100 $^{esfk}$
	beta_schedule	"linear" $^f$ , "quad" $^es$
	residual_layers	4 $^e$ , 8, 16 $^{sfk}$
	residual_channels	4 $^{sfk}$ , 8, 16 $^e$
	scaling	False, True $^{esfk}$
Data	History length to prediction length ratio	1 $^f$ , 2 $^{sk}$ , 3 $^e$
Training	Optimizer	Adam $^{esfk}$
	Learning rate	(10 $^{-4}$ ) $^f$ , (10 $^{-3}$ ) $^e$ , (10 $^{-2}$ ) $^{sk}$
	Gradient clipping	(10 $^1$ ), (10 $^2$ ) $^{sfk}$ , (10 $^4$ ) $^e$

The benchmark results for the CRPS-Sum and CRPS are respectively shown in tables 1 and 9.

**Table 9:** Means and standard deviations of the CRPS metrics on the backtesting benchmarks. The standard deviations are computed on both the various independant trials and the various backtesting timestamps (see §C.5).

Model	electricity	solar-10min	fred-md	kdd-cup
ETS	0.094 $\pm$ 0.040	0.844 $\pm$ 0.313	0.050 $\pm$ 0.035	0.560 $\pm$ 0.065
Auto-ARIMA	0.129 $\pm$ 0.052	0.636 $\pm$ 0.167	0.052 $\pm$ 0.022	0.477 $\pm$ 0.047
TempFlow	0.107 $\pm$ 0.078	0.601 $\pm$ 0.138	0.110 $\pm$ 0.010	0.461 $\pm$ 0.022
TimeGrad	0.101 $\pm$ 0.092	0.560 $\pm$ 0.193	0.142 $\pm$ 0.358	0.495 $\pm$ 0.116
GPVar	0.067 $\pm$ 0.032	<b>0.298 <math>\pm</math> 0.108</b>	0.086 $\pm$ 0.031	0.459 $\pm$ 0.030
TACTiS-GC	0.099 $\pm$ 0.039	0.334 $\pm$ 0.087	0.064 $\pm$ 0.036	<b>0.387 <math>\pm</math> 0.028</b>
TACTiS-TT	<b>0.054 <math>\pm</math> 0.020</b>	0.322 $\pm$ 0.142	<b>0.048 <math>\pm</math> 0.029</b>	0.414 $\pm$ 0.029

An alternative metric is the energy score (Gneiting & Raftery, 2007). Like the CRPS and CRPS-Sum metrics, it is a proper scoring method and thus a perfect forecast would minimize it. Unlike the CRPS and CRPS-Sum metrics, it is sensitive to the correlations between all forecasted variables, thus allowing a good multivariate forecasting technique to shine when compared to one which forecasts each series independently. The energy score is defined as:

$$\text{energy}(\{X, x\}) = \mathbb{E}_X \|X - x\|_F^\beta - \frac{1}{2} \mathbb{E}_{X, X'} \|X - X'\|_F^\beta, \quad (15)$$

where  $x$  is the observed value in matrix form,  $X$  and  $X'$  are two independent variables from the forecasted sampling process in matrix forms,  $\beta$  is a parameter set to 1, and  $\|\cdot\|_F$  is the Frobenius matrix norm.

The benchmark results for the energy score are shown in table 10. However, it should be noted that these results have been obtained from models in which hyperparameters were selected such as to minimize the CRPS-Sum and not the energy score. It is thus likely that some hyperparameters are not optimal in term of energy score, so these results may not be the best the models can do.

## D. Interpolation experiments

In this section, we evaluate the ability of TACTiS to perform interpolation, i.e., estimating the distribution of missing values for a gap *within* a time series.

**Table 10:** Means and standard deviations of the energy score metrics on the backtesting benchmarks. The standard deviations are computed on both the various independant trials and the various backtesting timestamps (see §C.5).

Model	electricity $\times 10^4$	solar-10min $\times 10^2$	fred-md $\times 10^5$	kdd-cup $\times 10^3$
ETS	$7.94 \pm 2.63$	$4.74 \pm 0.53$	<b><math>7.90 \pm 6.19</math></b>	$3.60 \pm 0.57$
Auto-ARIMA	$44.59 \pm 24.98$	$19.42 \pm 10.69$	$8.72 \pm 3.49$	$18.76 \pm 14.77$
TempFlow	$10.43 \pm 7.57$	$4.73 \pm 1.14$	$20.09 \pm 2.20$	$3.49 \pm 0.94$
TimeGrad	$9.69 \pm 9.28$	$4.31 \pm 1.29$	$19.87 \pm 45.01$	$3.30 \pm 0.85$
GPVar	$6.80 \pm 1.99$	<b><math>2.60 \pm 0.34</math></b>	$11.43 \pm 5.33$	$3.18 \pm 0.62$
TACTiS-GC	$8.70 \pm 3.17$	$2.94 \pm 0.27$	$9.55 \pm 6.17$	<b><math>2.65 \pm 0.51</math></b>
TACTiS-TT	<b><math>5.41 \pm 1.83</math></b>	$3.98 \pm 1.29$	$8.36 \pm 4.63$	$4.59 \pm 2.25$

**Data generation** In this experiment, we consider a univariate<sup>12</sup> time series generated according to the following stochastic volatility process (Kim et al., 1998):

$$y_t \mid h_t \sim \mathcal{N}(0, \exp h_t) \quad (16)$$

$$h_t \mid h_{t-1}, \mu, \phi, \sigma \sim \mathcal{N}(\mu + \phi(h_{t-1} - \mu), \sigma^2) \quad (17)$$

$$h_0 \mid \mu, \phi, \sigma \sim \mathcal{N}(\mu, \sigma^2 / (1 - \phi^2)), \quad (18)$$

with a log-variance of level  $\mu = -9$ , persistence  $\phi = 0.99$ , and volatility  $\sigma = 0.04$ . The  $h_t$  variables are unobserved and correspond to a latent time-varying volatility process. Our quantity of interest is  $x_t \stackrel{\text{def}}{=} x_{t-1} + y_t$ , where  $y_t$  is a stochastic increment incurred at each time step.

*Training data.* We use this process to generate a univariate time series  $\mathbf{x}^{\text{train}}$  of length 10,000, with  $x_1^{\text{train}} = 1$ . This time series is used to train TACTiS.

*Evaluation data.* We then generate 1000 more univariate time series, denoted  $\mathbf{x}_1^{\text{test}}, \dots, \mathbf{x}_{1000}^{\text{test}}$ , which correspond to possible trajectories of length 500 starting at the end of  $\mathbf{x}^{\text{train}}$ . For each  $\mathbf{x}_i^{\text{test}}$ , we create a gap of missing values of length 25 at an arbitrary time point. We then use the Markov Chain Monte-Carlo sampling capabilities of the Stan probabilistic programming language (Stan Development Team, 2022) to sample possible interpolation trajectories from the posterior distribution of missing values. Such trajectories form a ground truth for the interpolation task associated to  $\mathbf{x}_i^{\text{test}}$ .

**Training protocol** We train TACTiS using batches of 64 windows of length 125 drawn randomly from the training sequence  $\mathbf{x}^{\text{train}}$ . For each window, we mask the values of the center 25 time points and let the other time points (50 on each side) be observed. The model then learns to estimate the distribution of the 25 masked values given the 100 observed ones. The hyperparameter values used in this experiment are reported in Tab. 11.

**Evaluation protocol** For each of the evaluation time series  $\mathbf{x}_i^{\text{test}}$ , we extract a region of length 125 centered on the gap of missing values.<sup>13</sup> We then use TACTiS to draw samples from the estimated distribution of missing values. Then, the energy score (see Eq. (15)) is used to compare the sampled trajectories to *each* of the ground truth trajectories for  $\mathbf{x}_i^{\text{test}}$ . This results in a distribution of energy scores.

For comparison, we repeat the same process and obtain a distribution of energy scores for the following baselines:

- Oracle: an oracle model that produces samples by randomly drawing from the ground truth trajectories for  $\mathbf{x}_i^{\text{test}}$ .
- Dummy: a simple baseline that performs linear interpolation between the points directly before and after the gap of missing values. This baseline is deterministic, i.e., all its samples are identical.

We then use the Wasserstein distance to compare the distribution of scores obtained for TACTiS and for the Dummy baseline to that of the Oracle, for each testing series  $\mathbf{x}_i^{\text{test}}$ .

## Results and conclusions

Fig. 4 summarizes the Wasserstein distances obtained for each of the testing series. Clearly, the distributions estimated by

<sup>12</sup>We could also have considered a multivariate setting, but we limit the experiment to a univariate one for simplicity.

<sup>13</sup>We keep only the testing tasks where such sampling was within the bounds of the time series, resulting in 803 valid tasks  $\mathbf{x}_i^{\text{test}}$ .

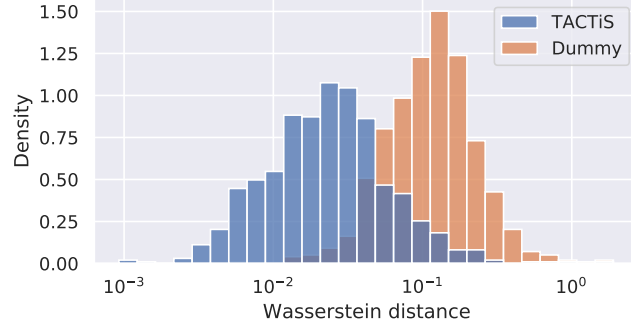


**Figure 4:** TACTiS outperforms the Dummy baseline on the considered interpolation tasks, as shown by the distribution of Wasserstein distances between the energy score distributions of each baseline and the Oracle (estimated for our 803 valid testing tasks). The TACTiS and Dummy distributions have means at 0.0391 and 0.1459, respectively. The distances are estimated using 50 samples from each energy score distribution.

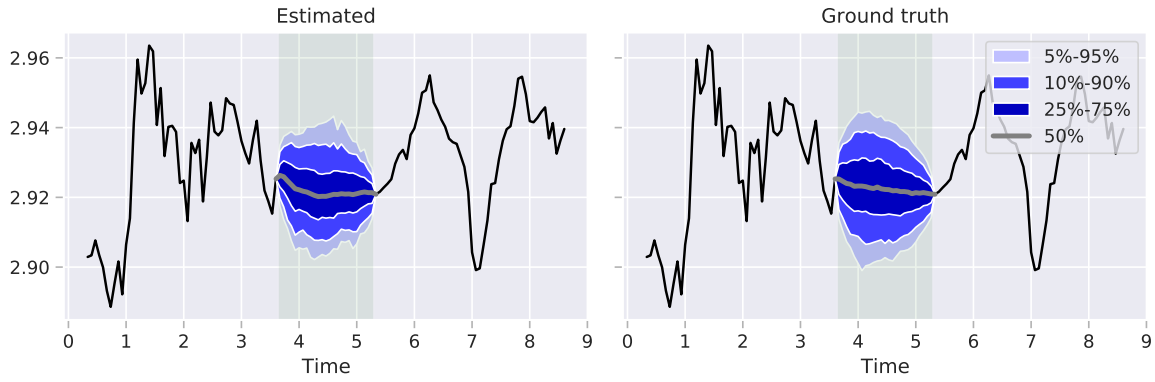


**Figure 5:** Interpolation - Good performance. Comparison of the interpolation distribution estimated by TACTiS (left) and the ground truth distribution (right) for the task where TACTiS most faithfully approximates the Oracle, as measured by the Wasserstein distance between energy score distributions ( $WD = 0.0009$ ). The colors correspond to confidence intervals of the distribution. All distributions are estimated using 1000 samples.

TACTiS are closer to the ground truth distributions than those estimated by the Dummy baseline. This is reflected in their respective Wasserstein distance distributions, which have a mean of 0.0391 and 0.1459 for TACTiS and the Dummy baseline, respectively. We further assess the quality of the distributions estimated by TACTiS visually. Fig. 5 compares the distribution estimated by TACTiS for the task ( $x_i^{\text{test}}$ ) where the energy score distribution was closest to that of the Oracle ( $WD = 0.0009$ ). We observe that the shape of the estimated distribution is very close to that of the ground truth. Furthermore, its median is coherent with the values observed directly before and after the gap. We repeat this analysis for the task where the WD was closest to the mean of the TACTiS WD distribution ( $WD = 0.0388$ ) and show the results in Fig. 6. The same conclusions apply, supporting the fact that TACTiS generally performs well at this interpolation task. Finally, we repeat the analysis for the task where the WD was maximal ( $WD = 1.4578$ ) and show the results in Fig. 7. In this case, TACTiS clearly fails to estimate an upwards trend in the median of the ground truth distribution, leading to a median that is not coherent with the bounds of the gap. Fortunately, tasks where TACTiS performs at this level are rare, as supported by the distribution of Wasserstein distances.

In conclusion, the aforementioned results clearly show the ability of TACTiS to perform accurate probabilistic interpolation. It is thus safe to conclude that TACTiS is sufficiently flexible to address both forecasting and interpolation tasks.

## E. Forecasting examples

In this section, we present a few examples of the probabilistic forecasts generated by TACTiS-TT in our backtesting experiments. Due to the dimensionality of the datasets, it is infeasible to show all forecasts, so we selected a few examples to demonstrate both the strength and weakness of TACTiS-TT. For each dataset, we thus hand-picked 4 particularly good forecasts from the experi-

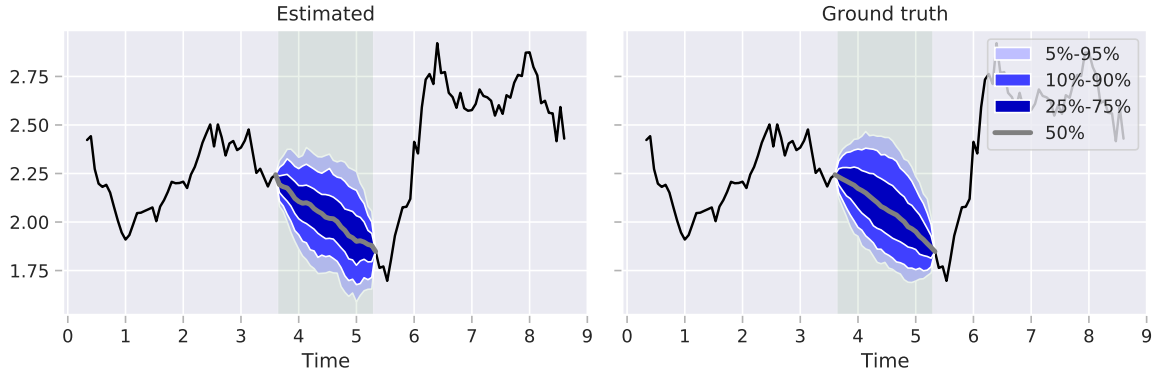


**Figure 6:** Interpolation - Average performance. Comparison of the interpolation distribution estimated by TACTiS (left) and the ground truth distribution (right) for a task that is representative of the average performance of TACTiS, as measured by the Wasserstein distance between energy score distributions ( $WD = 0.0388$ ). The colors correspond to confidence intervals of the distribution. All distributions are estimated using 1000 samples.

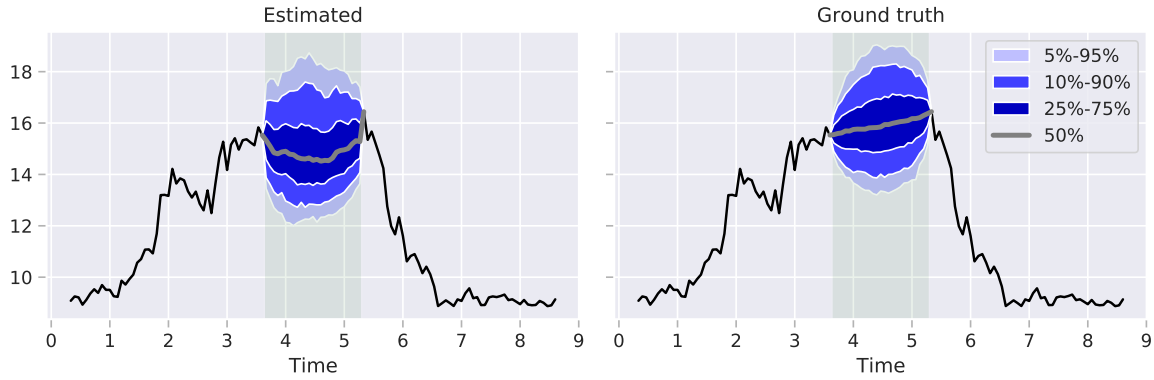


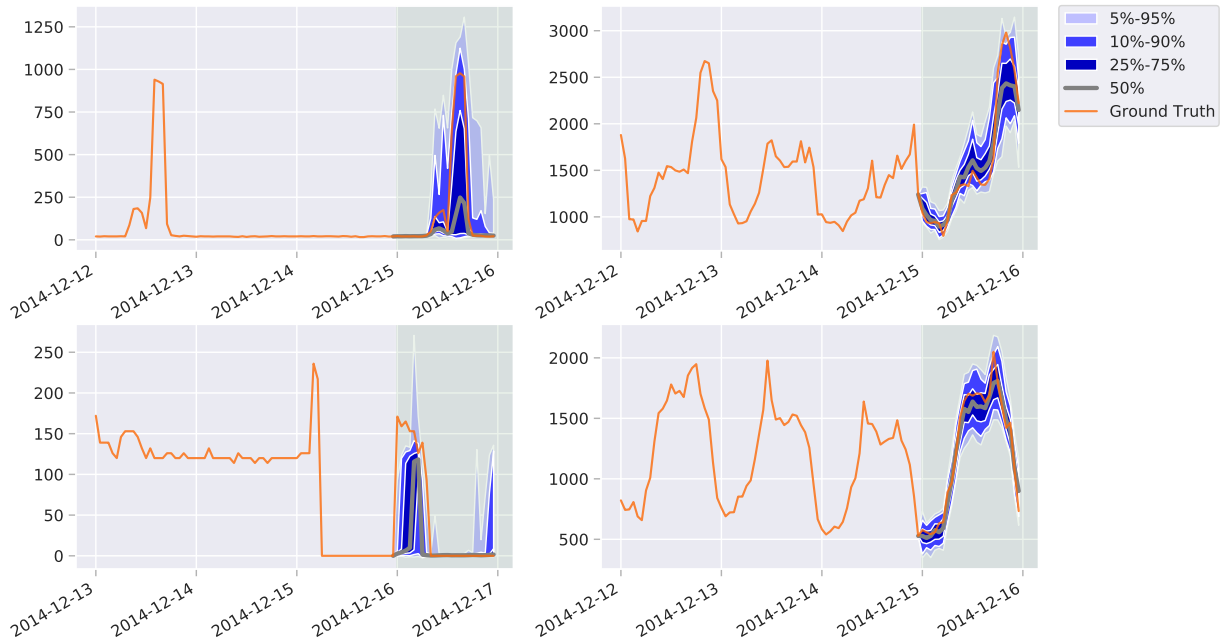
**Figure 7:** Interpolation - Poor performance. Comparison of the interpolation distribution estimated by TACTiS (left) and the ground truth distribution (right) for the task where TACTiS least faithfully approximates the Oracle, as measured by the Wasserstein distance between energy score distributions ( $WD = 1.4578$ ). The colors correspond to confidence intervals of the distribution. All distributions are estimated using 1000 samples.

ment with the lowest CRPS-Sum score, and 4 particularly bad forecasts from the experiment with the highest CRPS-Sum score.

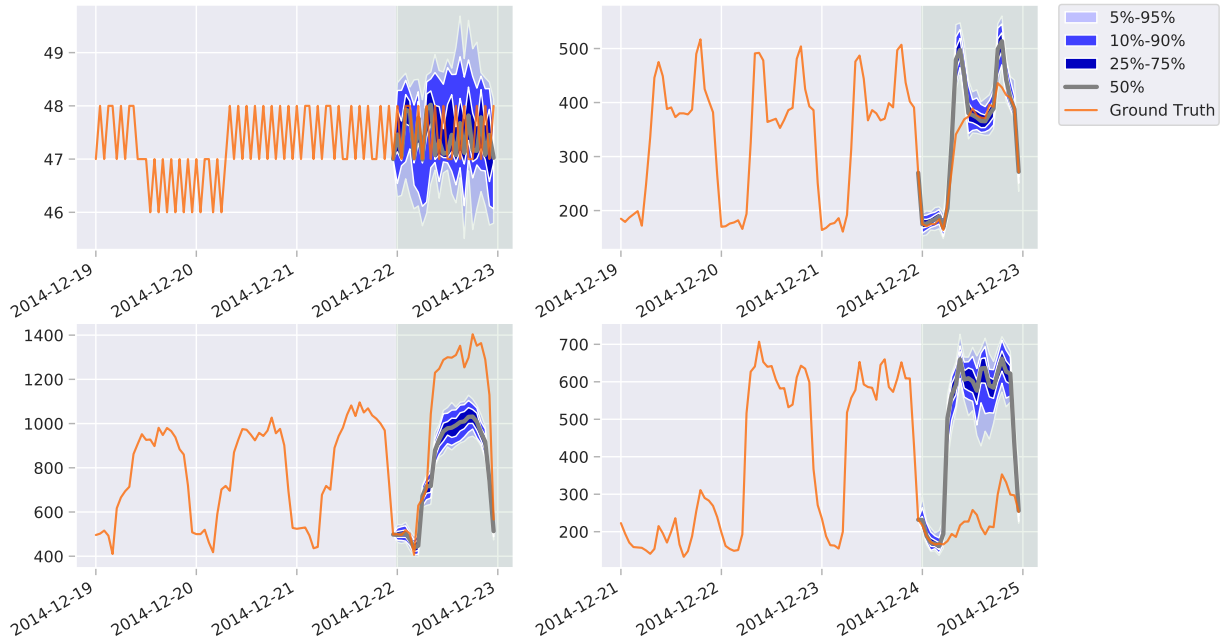
Fig. 8 shows some particularly good forecasts for the electricity dataset. The top-left and bottom-left forecasts show that the model was able to predict that the time series could see a sudden increase after a zero-valued range. The top-right and bottom-right forecasts show the model’s ability to follow the daily periodicity of the data. The top-right forecast is particularly impressive since was able to follow the Monday pattern after lower values for Saturday and Sunday since the time embedding used in our experiments did not have any week-of-day information.

Fig. 9 shows some particularly bad forecasts for the electricity dataset. The top-left forecast has relatively uniformly spread values, even though the data has only 3 possible values, thus showing a limit to the flow’s ability to fit discrete distributions, especially if only a small number of series have discrete patterns. The top-right forecast has the model being extremely confident that the series would have the same pattern in the prediction range as in the previous days, missing the change in behavior. The bottom-left one is similar, the model predicting a similar day and missing the increasingly fast increase from day-to-day. The bottom-right forecast also shows the model assumes that the series has daily periodicity, even though it was shown that lower values could happen in the history.

Fig. 10 shows some particularly good forecasts for the solar-10min dataset. The top-left and top-right forecasts show why the model must give a large range of possible values in its forecasts: even for quite similar historical values, the data to be forecasted can suddenly jump, or have a tamer behavior. The bottom-left and bottom-right forecasts are forecasts which start when the series is non-zero. One particular aspect of these forecasts is that they have a large variance from the first time



**Figure 8:** Hand-picked example forecasts for the electricity dataset. These examples have been selected to show particularly **good** forecasts. The historical ground truth shown is the one that was made available to the model. Note that the data is from 2014, so December 15th is a Monday.



**Figure 9:** Hand-picked example forecasts for the electricity dataset. These examples have been selected to show particularly **bad** forecasts. The historical ground truth shown is the one that was made available to the model.

**Table 11:** Hyperparameters for TACTiS for the interpolation experiment.

	Hyperparameter	Selected value
Model	Encoder transformer embedding size (per head) and feed forward network size	8
	Encoder transformer number of heads	2
	Encoder number of transformer layers	2
	Encoder time series embedding dimensions	5
	Decoder MLP number of layers	1
	Decoder MLP hidden dimensions	8
	Decoder transformer number of heads	2
	Decoder transformer embedding size (per head)	8
	Decoder number transformer layers	2
	Decoder number of bins in conditional distribution	20
	Decoder DSF number of layers	2
	Decoder DSF hidden dimensions	8
	Dropout	0
Data	Normalization	Standardization
	History length to prediction length ratio (before interpolation range)	2
	History length to prediction length ratio (after interpolation range)	2
Training	Optimizer	RMSprop
	Learning rate	$10^{-3}$
	Weight decay	$10^{-5}$
	Gradient clipping	$10^3$

step, which is unusual. This is necessary since, for this dataset, the values can quickly change in a single time step, as seen in the bottom-left figure.

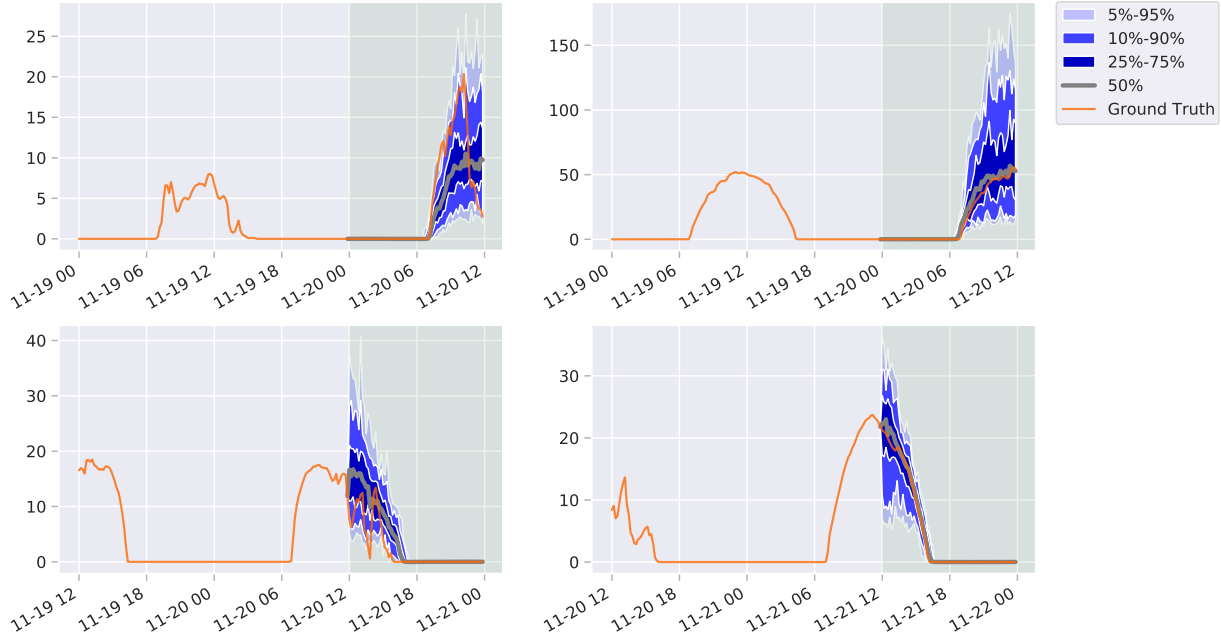
Fig. 11 shows some particularly bad forecasts for the `solar-10min` dataset. All four of these forecasts have the same failure mode, which is to have missed that the data could go as low as it did in the ground truth.

Fig. 12 shows some particularly good forecasts for the `fred-md` dataset. They show that the model can predict data with a variety of trends. Furthermore, the variance of the forecast gradually increase as we get further and further from the historical values. The ground-truth values stay in the forecasted range, but not always near the median, thus showing that the variance is not overestimated.

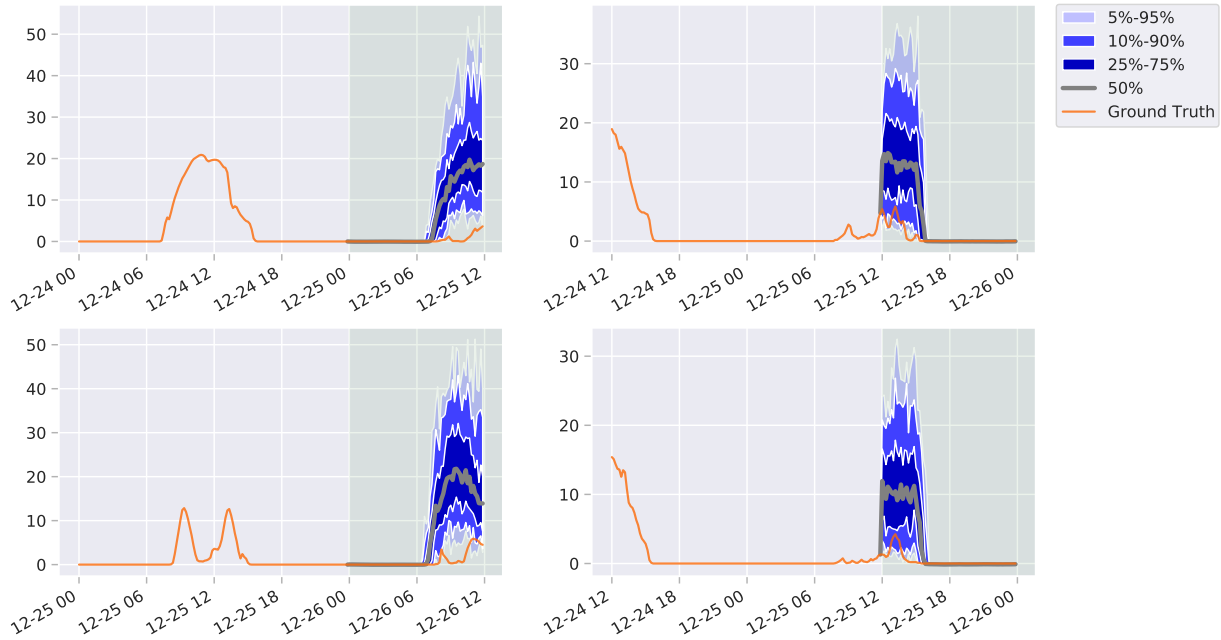
Fig. 13 shows some particularly bad forecasts for the `fred-md` dataset. The top-left and top-right forecasts show that the model leaned too hard on the historical trend, and overacted to a blip in the data (top-left) or missed a change in the trend (top-right). The bottom-left and bottom-right forecasts are more dramatic since the model totally missed radical changes in the behavior of the series.

Fig. 14 shows some particularly good forecasts for the `kdd-cup` dataset. All four of them are quite similar, in that the model must predict relatively uniform ranges in possible values, which are shown to be accurate when looking at the oscillations from the ground truth. Furthermore, we can see the variance increase gradually near the history, unlike for the `solar-10min` dataset, thus showing that the model learned that the `kdd-cup` dataset has less rapid shifts in its values.

Finally, Fig. 15 shows some particularly bad forecasts for the `kdd-cup` dataset. The top-left and top-right forecasts show that the model underestimated how high the series could reach, not having seen such values in the history. The bottom-left is the opposite, the model having underestimated the odds of the series staying at relatively constant and low values. The bottom-right shows two distinct failures: first, the model expected the series to stop being constant after a long constant period; second, the model thought it possible that the series could go negative, even though the `kdd-cup` dataset is strictly non-negative.



**Figure 10:** Hand-picked example forecasts for the solar-10min dataset. These examples have been selected to show particularly **good** forecasts. The historical ground truth shown is the one that was made available to the model.



**Figure 11:** Hand-picked example forecasts for the solar-10min dataset. These examples have been selected to show particularly **bad** forecasts. The historical ground truth shown is the one that was made available to the model.

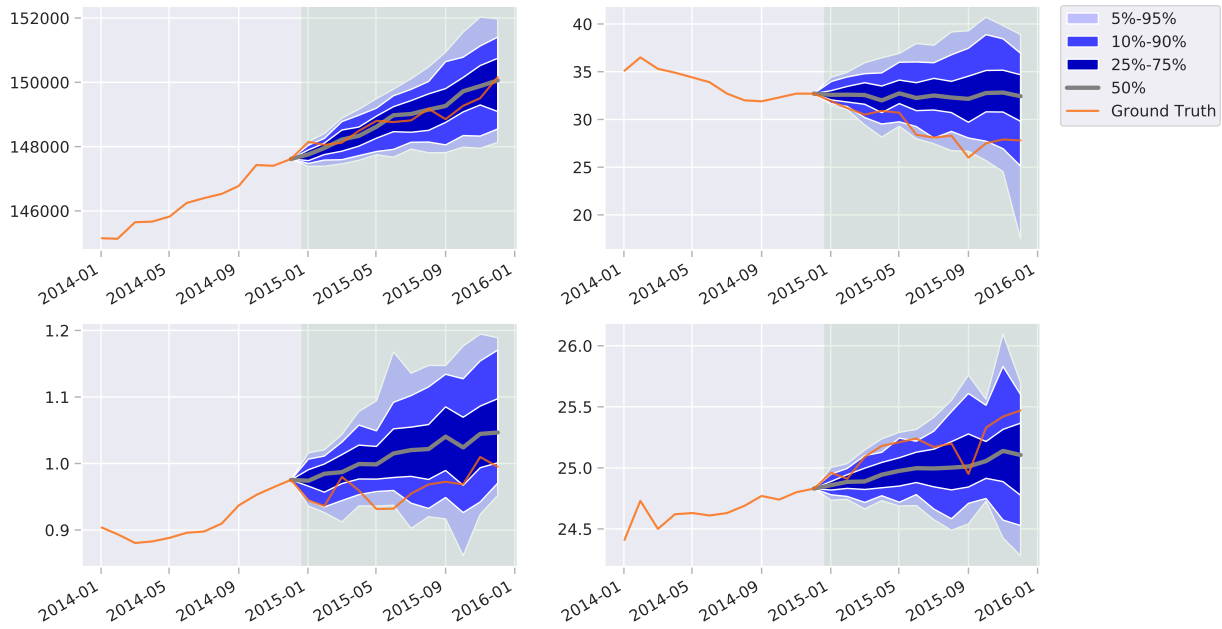


**Figure 12:** Hand-picked example forecasts for the fred-md dataset. These examples have been selected to show particularly **good** forecasts. The historical ground truth shown is the one that was made available to the model.

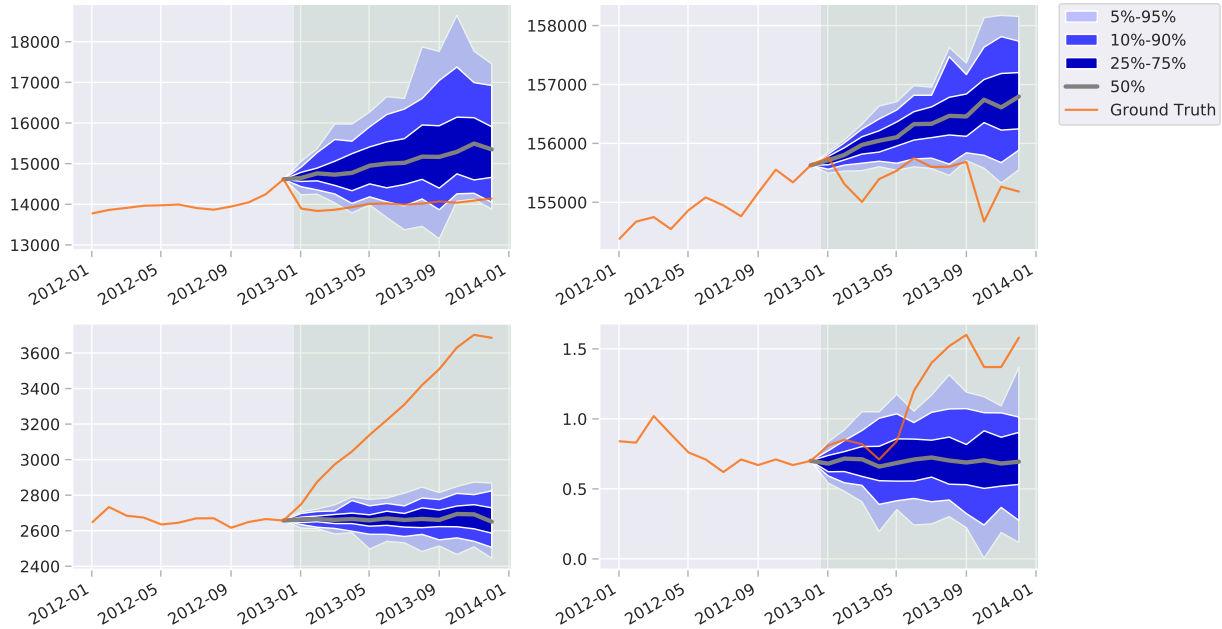


**Figure 13:** Hand-picked example forecasts for the fred-md dataset. These examples have been selected to show particularly **bad** forecasts. The historical ground truth shown is the one that was made available to the model.

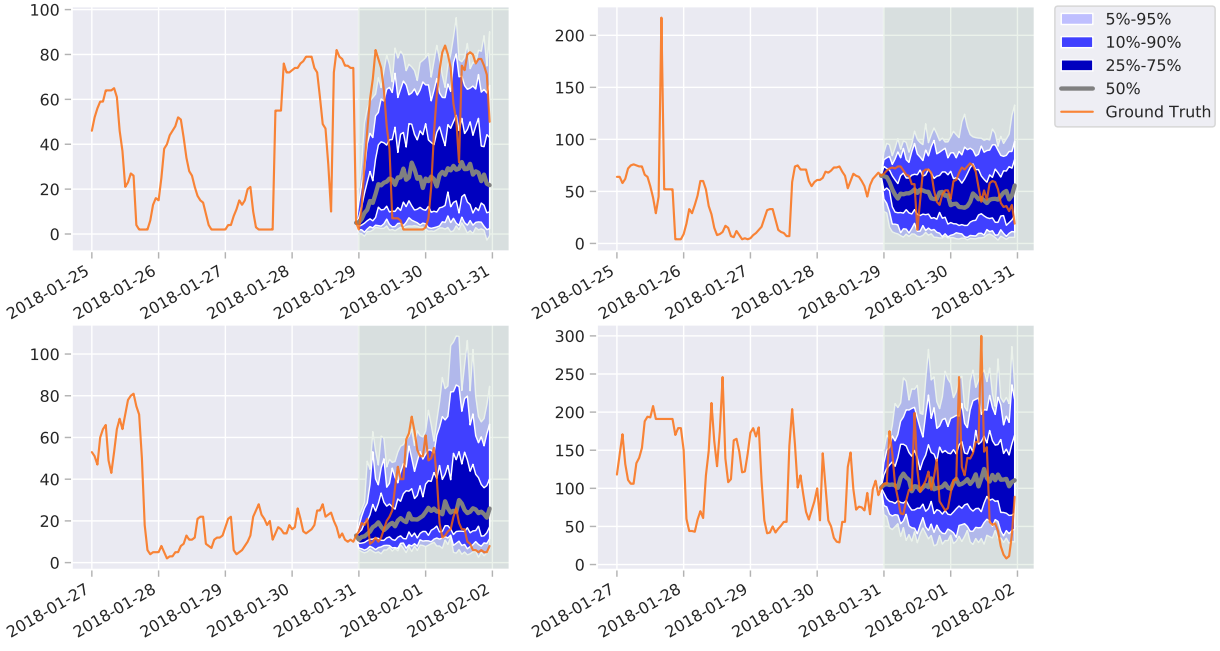


**Figure 14:** Hand-picked example forecasts for the kdd-cup dataset. These examples have been selected to show particularly **good** forecasts. The historical ground truth shown is the one that was made available to the model.

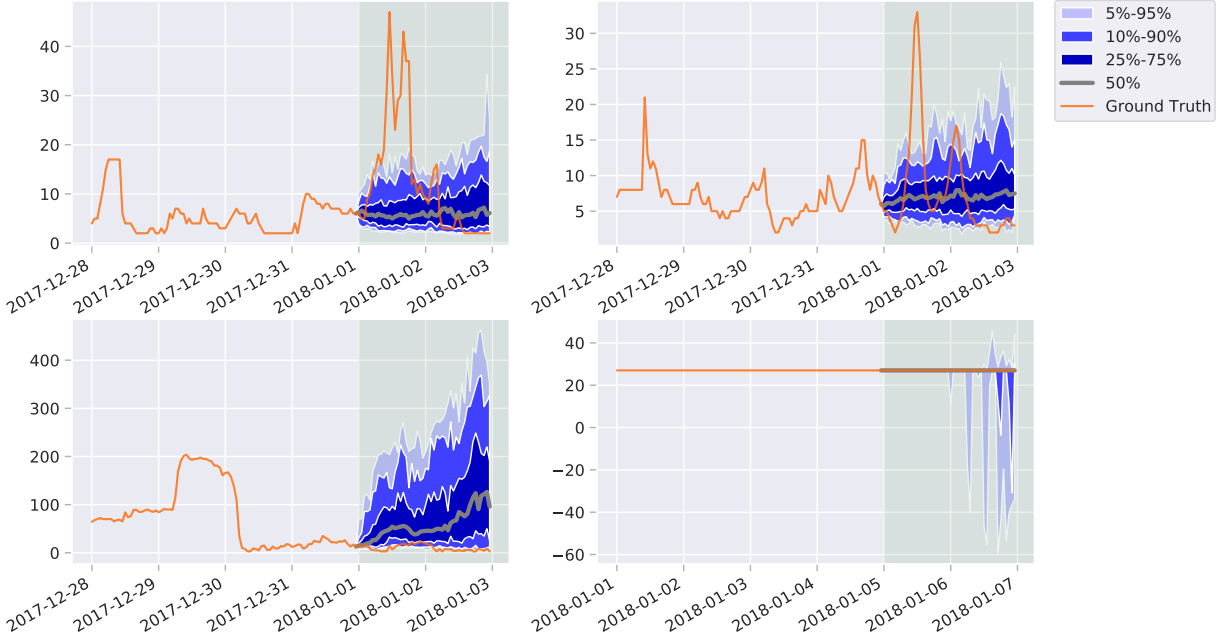


**Figure 15:** Hand-picked example forecasts for the kdd-cup dataset. These examples have been selected to show particularly **bad** forecasts. The historical ground truth shown is the one that was made available to the model.